Spatial and Temporal Evolution of the Foredune Restoration Project at Terschelling, The Netherlands

Master Thesis submitted for the Earth Surface and Water program

Utrecht University, Department of Physical Geography

Kees van der Meulen

Newly forming dunes at middle Terschelling, the Netherlands, between RSP 15 and 20 (Stuivende duinen, n.d.).

Supervisors:

prof. dr. Gerben Ruessink

dr. Wiebe Nijland

Utrecht, July 2024

Abstract

Coastal management practices intended to strengthen established foredunes have contributed to the stabilization of coastal ecosystems. As a result, the biodiversity within these ecosystems, as well as their ability to grow with rising sea levels, declined. To counteract these adverse trends, some coastal management projects nowadays aim to restore dynamics in coastal ecosystems through the excavation of foredune notches, gaps in the most seaward dune that resemble naturally occuring trough blowouts. It is essential to understand how these restoration measures effect the spatio-temporal evolution of the coastal ecosystem. However, knowledge regarding the physical-ecological interactions that influence the evolution of restored coastal ecosystems, especially after initial developments, is limited. Using annual lidar data and freely available Landsat and Sentinel-2 satellite imagery, this study examines the development of a coastal dunefield at Terschelling, the Netherlands, where sand trapping fences were removed and notches were excavated through a 5-km long unvegetated foredune in 1995. The results reveal that the restoration measures initially led to remarkable dynamism, with sand surface areas gaining ~2.85 ha/yr on average and absolute sand volume change rates reaching up to ~7.1×10^5 m^3/yr. The unvegetated rolling foredune eroded and new foredunes and transgressive sand sheets were gradually formed. As sand deposition on and seaward of the new foredunes limited sand transport towards the hinterland, aeolian erosion formed deflation basins between the new foredunes and transgressive sand sheets. Vegetation primarily re-established in the deflation basins, at elevations below 3 m mean sea level, near the water table, where depositional and erosional rates were below 0.3 and 0.1 m/yr, respectively. Once established, vegetation spread to higher elevations. The results indicate that vegetation growth within the dunefield is mainly regulated by the geomorphological evolution, dynamism and topography of the dunefield. Furthermore, the findings indicate that the dunefield will restabilize completely. Proactive measures such as repeated excavation may be required to reintroduce dynamism.

Keywords

Foredune; Blowouts; Dune stabilisation; Dune remobilisation; Physical-ecological feedbacks; Google Earth Engine; LiDAR

Contents

1. Introduction

Coastal dunes are aeolian landforms that are found at almost all geographical latitudes along the shorelines of marine water bodies (Martínez and Psuty, 2004). To humankind, coastal dunes are of great importance by, for example, safeguarding low-lying areas against marine flooding (e.g., Keijsers, et al., 2015) and serving as a source of drinking water (e.g., van Dijk, 1989; Van der Meulen and Salman, 1996). Beyond their benefits to humankind, coastal dunes serve as ecological habitats accommodating a rich array of species, thereby contributing to widespread ecological diversity (e.g., Bakker and Stuyfzand, 1993; Martínez and Psuty, 2004).

During the last century, coastal management has primarily been focusing on strengthening and stabilizing coastal foredunes in order to protect low-lying areas against the sea (e.g., Provoost et al., 2011; Hanley et al., 2014; Gao et al., 2020). To stabilize bare sand surfaces and stimulate vegetation succession, coastal protection measures often included planting vegetation and placing sand trapping fences (e.g., Nordstrom and Arens, 1998; Hesp and Hilton, 2013). These measures have greatly increased foredune volumes and heights, and transformed many mobile dune systems into anthropogenically modified and stabilized dunes. By acting as a barrier to aeolian transport, the increased height of stabilized foredunes greatly reduce aeolian sand transport from the beach into the back dunes, preventing them from growing (e.g., Keijsers et al., 2015; Provoost et al., 2011). Stabilized coastal ecosystems therefore possess a reduced biodiversity (Martinez et al., 2013) and are unlikely to be adaptive to sea level rise (Arens et al., 2013; Osswald et al., 2019).

Recognizing the drawbacks of dune stabilization, coastal managers nowadays believe that the remobilization of stabilized coastal ecosystems is crucial to restore biodiversity and protect coastal areas against future sea level rise (e.g., Martinez et al., 2013; Arens et al. 2013). The general idea of dune remobilization is that natural processes will maintain biodiversity levels through erosion, providing opportunities for pioneer species, and through the burial of sand, destroying vegetation (e.g., Arens et al., 2004, 2013). The current Dutch dune remobilization strategy is the excavation of notches in the foredune, resembling naturally occuring trough blowouts (e.g., Arens et al., 2004, 2013). One of the first experiments attempting to restore aeolian processes and remobilize the coastal system started in 1995 on Terschelling, one of the Dutch barrier islands (e.g., POK, 1998; Arens et al., 2007; Van der Valk et al., 2013; Rijkswaterstaat, 2014). By removing sand trapping reeds and excavating foredune notches, the experiment aimed to reconnect the back dunes with the beach-foredune system (e.g., Arens et al., 2013). While the restoration measures initially led to and sand transport hundreds of meters inland (e.g., POK, 1998; Arens et al., 2007; Rijkswaterstaat, 2014), recent observations indicate that dynamics within the dunefield are declining, and that vegetation is re-establishing.

Excavated foredune notches at Terschelling and other locations have already been proven to act as effective channels for aeolian transport into the back dunes (e.g., Arens et al., 2007; Van der Valk et al., 2013; Ruessink et al., 2018; Laporte-Fauret et al., 2021, 2022). However, there is limited understanding regarding the physical-ecological feedback mechanisms that shape their spatio-temporal evolution. Using airborne lidar data and satellite imagery, this study aims to unravel how these feedback mechanisms influence the recent morphological changes of the

remobilized dunefield at Terschelling. Due to the global rise in sea level and the increasing coastal population, the risk of coastal flooding will intensify if adaptive measures are not implemented (e.g., Nicholls, 2002; Hanley et al., 2014). Given that coastal mobility is crucial for coastal transgression and resilience against sea-level rise (e.g., Pelletier et al, 2015; Arens et al., 2013), research on coastal mobility restoration projects is essential.

2. Background

2.1. Coastal dunes

This section provides comprehensive background information on the initiation, dynamics, morphology and evolution of coastal foredunes, blowouts, parabolic dunes and transgressive sand sheets. For more extensive reviews on these dune types, see Hesp (1989, 2002, 2024) and Hesp and Walker (2013).

2.1.1. Foredunes

Foredunes are dune ridges aligned parallel to the coastline and represent the most seaward extend of the coastal dune system (Hesp, 2002; Martínez and Psuty, 2004). New foredunes, also know as incipient or embryo dunes, can initiate when aeolian sand transport is captured and deposited by rhizome growth, individual plants, vegetated patches or debris on the backshore, the area of the beach that is located between the high tide and landward limit of the beach (Hesp, 1989, 2002; Hesp and Walker, 2013). The spatiotemporal development and morphology of incipient foredunes depend mainly on the plant density and height, rates of transport and wind velocity (Hesp 2002; Hesp and Walker, 2013). While tall vegetation species and high wind velocities will result in narrow and high dune morphologies, lower vegetation species and low wind velocities result in lower and wider morphologies. In general, the potential sediment accumulation increases with increasing plant cover density, and higher rates of sediment transport will result in faster growth. Too high rates of sand accumulation, however, can suffocate vegetation (e.g., Hesp 2002; Hesp and Walker, 2013; Keijsers et al., 2015).

When incipient foredunes increase in height and volume, they evolve into established foredunes (Hesp, 2002; Hesp and Walker, 2013). Although established foredunes are often characterized by secondary plant species, the pioneer species that initiate the formation of the incipient foredunes can also dominate established foredunes. Established foredunes are therefore typically distinguished from incipient foredunes by a greater morphological complexity, size age, and position within the coastal system (Hesp, 2002; Hesp and Walker, 2013). The spatiotemporal evolution of an established foredune depends on sand supply, vegetation growth and wind and wave energy, as well as beach width and retro/progradation rate of the coast (Hesp, 2002; Hesp et al., 2016). Based on their morphology, established foredunes can be classified in five evolutionary stages (*Figure 1*; Hesp 2002). Stage 1 and 2 foredunes develop on stable or prograding coasts and are characterized by a high vegetation cover and positive sediment supply. When the coastal system retrogrades (erodes), the foredune develops towards stage 3. This stage is characterized by erosion and landward movement of the foredune. Stage 4 and 5 foredunes develop on highly erosional shores, and are characterized by remnant knobs of dune, and bare sand sheets. Possible evolutionary scenarios are illustrated in Figure 1, box A-D.

Wind flow dynamics and sand transport over foredunes depend on foredune topography and vegetation (e.g., Arens et al., 1995; Hesp et al., 2005). When onshore wind encounters a foredune, its flow is accelerated due to the topographic increase in foredune height. Generally, the wind flow increases as the height of the foredune increases. However, as wind flow encounters more vegetation on the foredune, the so-called roughness length of the foredune surface also increases. The increase in roughness length eventually surpasses the wind flow acceleration

effect of the topography (e.g., Arens et al., 1995). Due to variations in vegetation (e.g. height and density) and meteorological factors (e.g. general wind direction and speed), the maximum foredune height over which sand can be transported can be different per coastal region. Measurements by Arens et al. (1995) on three foredunes located in the Netherlands showed that maximum acceleration of wind flow on the foredunes occurs when foredune height increases up to 10 m MSL, and where the foredunes reached heights over 20 m MSL, sand transport does not reach the dune crest. While a foredune can prevent sediment transport inland, sand can still be transported inland via blowouts (*Figure 1, box B and C*).

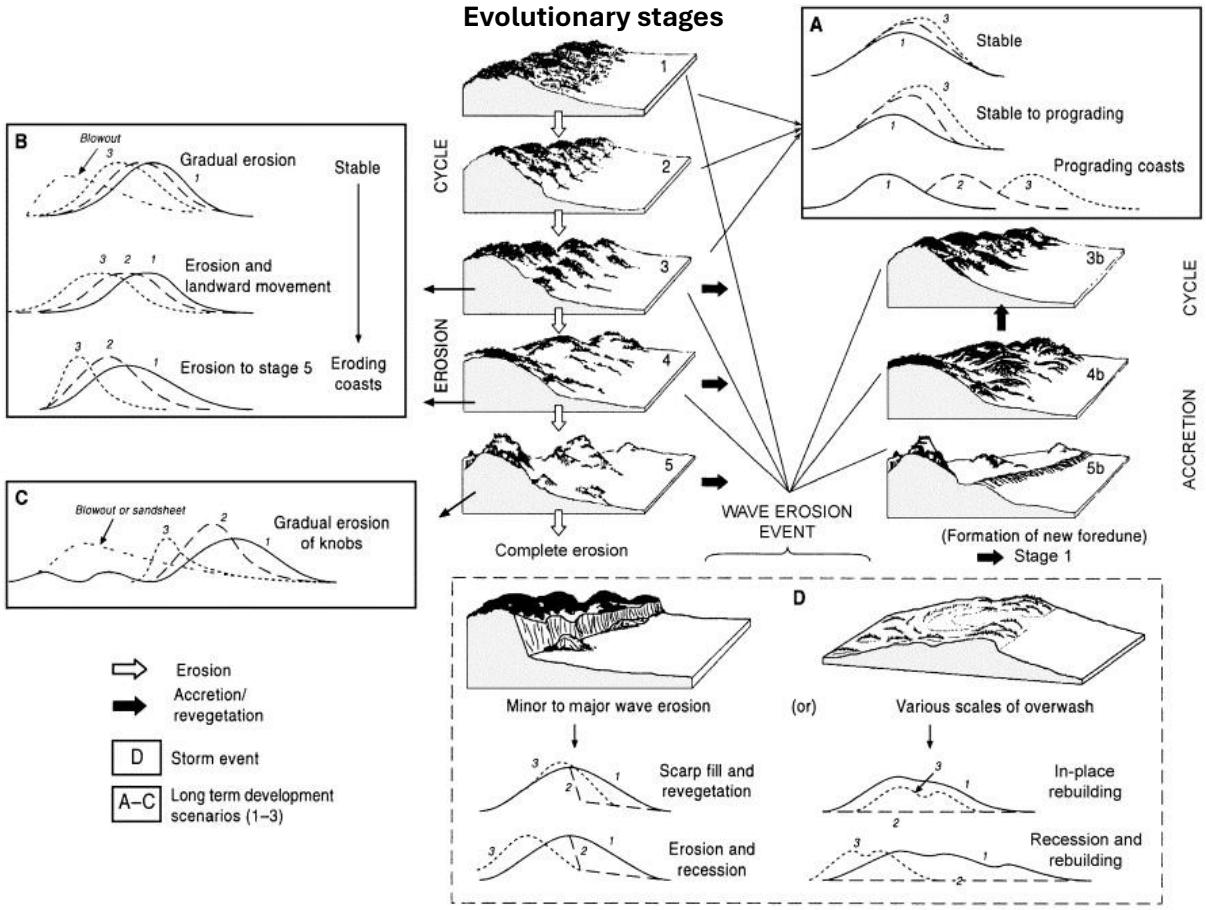

Figure 1. Established foredune development model by Hesp (2002). Numbers 1-5 indicate the five evolutionary stages of established foredunes based on their morphology. Possible foredune evolutionary pathways on stable/prograding [box A] and retrograding [box B and C] shores, as well as foredune evolution after a destructive wave erosion event [box D], are also displayed in the figure.

2.1.2. Blowouts

Blowouts are coastal features that naturally form in coastal environments (e.g., Sawakuchi et al., 2008; Jewell et al., 2017), where wind and wave energy is high, or in areas where beaches and foredunes undergo frequent erosion or recession (*Figure 1, box B and C*; Hesp, 2002). Blowouts are also artificially created as part of dune mobility projects (e.g., Arens et al., 2007; Ruessink et al., 2018; Laporte-Fauret et al., 2021). Based on their shape and characteristics, blowouts are commonly classified into two types, namely, saucer and trough blowouts. Saucer blowouts (*Figure 2A*) are characterized by a relatively shallow deflation basis, low erosional walls, and semicircular or saucer shape. Trough blowouts (*Figure 2B*) are characterized by a relatively deep

deflation basis, high erosional walls, and an elongated shape. The maximum depth of the deflation basin within a blowout is generally determined by the level of the water table or possible hard underlying layers (e.g., Gares, 1992; Hesp et al., 2016). Topographic flow acceleration within the deflation basin of trough blowouts can accelerate wind speeds up to two times the regional wind speed (Hesp and Hyde, 1996).

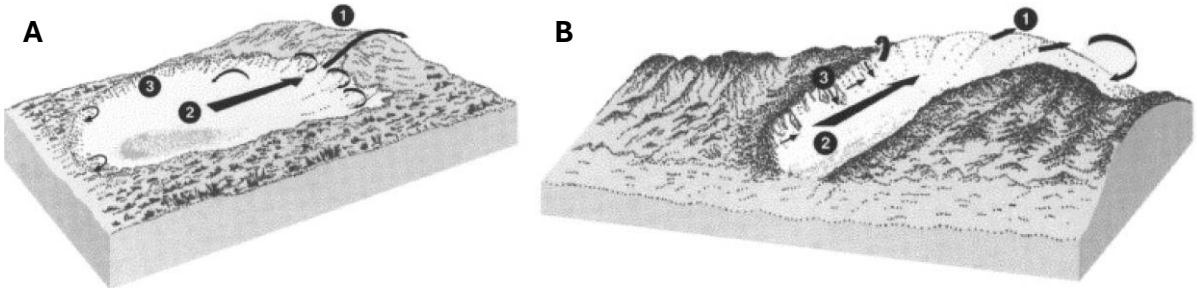

Figure 2. The morphology of a (A) saucer and a (B) trough blowout, illustrated by Hesp et al. (2002). Numbers indicate the (1) depositional lobe, (2) deflation basin and the (3) erosional walls. Typical wind flow through the blowouts is indicated with arrows.

Blowouts naturally initiate due to wave erosion, wind erosion, local wind flow acceleration, or a combination of these processes (Hesp, 2002; Hesp and Walker, 2013; Hesp et al., 2016). For example, when wave erosion destabilizes or breaches a dune, the topographical flow acceleration through the depression can stimulate wind erosion and develop a blowout. When vegetation cover in a dune is reduced due to animal grazing (e.g., Blanco et al., 2008), for example, wind erosion and subsequent flow acceleration can also result in blowout development.

The spatio-temporal evolution of a blowout mainly depends on vegetation growth, wind speed and direction, and retro/progradation rate of the coast (Hesp, 2002; Hesp and Walker, 2013). The evolution and geomorphological development are driven by feedbacks between physical (abiotic) and ecological (biotic) processes and can be divided into the geomorphological, bio-geomorphological and ecological stages (*Figure 3*; Schwarz et al., 2019). The first (*Geomorphological*) stage of blowout development is characterized by predominantly physical (erosional) processes, causing the blowout deflation basin depth and width to increase. As the blowout increases in size, the airflow through the blowout eventually reduces, resulting in a decrease in physical processes and an increase in ecological processes (vegetation growth). When feedbacks between ecological and physical processes are in balance, the second (Bio-geomorphological) stage is reached. If ecological processes dominate and the blowout deflation basin becomes vegetated, the final (*Ecological*) stage of the blowout is reached. This stabilization can be the result of incipient foredunes establishing seaward of the blowout deflation basin (e.g., Jewell et al., 2017), but can also be caused by high moisture levels that reduce erosion and stimulate vegetation establishment, or vegetation growth on the margins of the depositional lobe (Hesp, 2002; Hesp and Walker, 2013). Blowouts can increase in size and evolve into parabolic dunes (e.g., van Kuik et al, 2022), eventually becoming vegetated and stabilized blowouts (e.g., Jewell et al., 2017). Previous studies (e.g., Gares and Nordstrom, 1995; Jewell et al., 2017; van Kuik et al., 2022) have shown that blowout succession does not advance linearly through the stages. Observations by Jewell et al. (2017), for example, demonstrated that storm events can reactivated blowout systems. The complex development of trough blowouts, influenced by

nonlinear physical-ecological feedbacks and varying meteorological forces over time, can result in blowout lifetimes lasting for multiple decades (e.g., van Kuik et al., 2022).

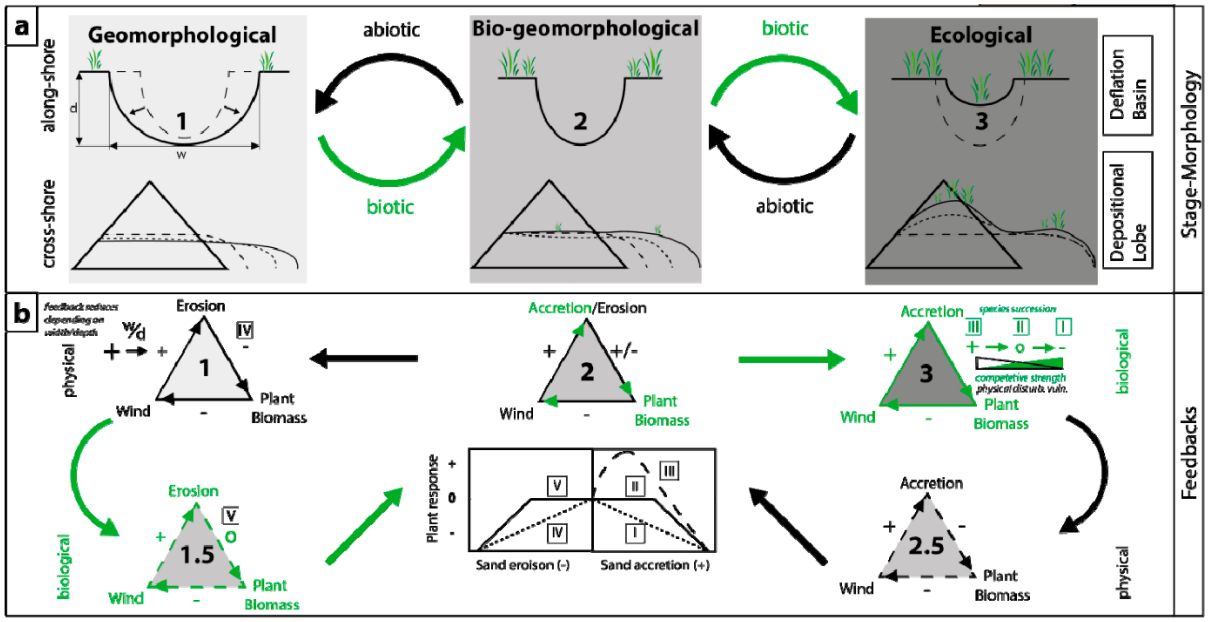

Figure 3. Three-stage conceptual model of blowout development by Schwarz et al. (2019). Per stage, both the (A) morphology of the depositional lobe and the deflation basin and (B) the physical and biological feedbacks are presented in the model.

2.1.3. Transgressive dunefields

Transgressive dunefields and smaller scale sand sheets, also known as migrating dunes (e.g., Olson and Van der Maarel, 1989), are sand deposits formed by sand migrating over a (partly) vegetated landscape (Hesp, 2024). Within a transgressive dunefield, landforms such as barchan dunes, blowouts, parabolic dunes and deflation basins can form (Hesp and Walker, 2013). When transgressive dunefields are active, they are (predominantly) unvegetated. When transgressive dunefields become less active, trey become vegetated (Hesp and Walker, 2013; Hesp, 2024). Transgressive dune sheets primarily initiate in regions with high sediment supply and high wind- and wave energy, limiting vegetation growth. Transgressive dune sheets also initiate on coast experiencing erosion, or on coast where vegetation is destructed by human actions, fires, or grazing animals. Additionally, the merging of parabolic dunes can also lead to the formation of transgressive dunefields (Hesp and Walker, 2013; Hesp 2024).

The development of the transgressive dunefield is mainly dependant on the sediment supply. Three different evolutionary patterns of transgressive dunefield development have been described by Hesp (2013). In cases of very high sediment supply, continuous sediment deposition on the beach and dunes supports the ongoing development of an active transgressive dunefield (pattern 1). If sediment supply slows down (temporarily), the dune field may migrate landwards, depending on the dominant wind regime. This movement can result in the formation of a deflation plain or basin (*Figure 4A*) on the seaward side of the transgressive dunefield (pattern 2). When a transgressive dunefield keeps migrating, the dunefield can evolve into parabolic dunes (*Figure 4B*). When the sediment supply increases, a second transgressive dune sheet can form

(pattern 3). This process can be repeated, developing multiple (overlaying) transgressive dunefields over time.

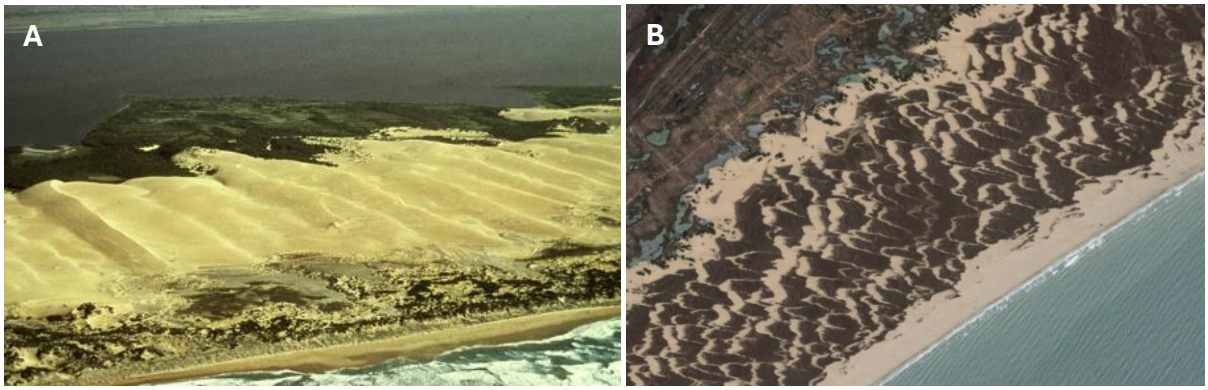

Figure 4. (A) Deflation basin that formed seaward of the transgressive dunefield, South Australia, and (B) a transgressive dunefield and parabolic dunes that have evolved from the transgressive dunefield at the Sao Fransisco delta, Brazil. Both images are from Hesp (2013).

2.1.4. Parabolic dunes

Parabolic dunes are hollow shaped dunes that have U- or V-shaped depositional lobes, tapering to the windward side (*Figure 4B*; Hesp and Walker, 2013). Similar to blowouts, the deflation basin of parabolic dunes can continue to erode until a base level such as the water table or a hard underlying layer is reached (Hesp and Walker, 2013; Hesp, 2024). Parabolic dunes mostly initiate on coast with high wind and wave energy that have a large supply of sediment (Hesp, 2024). Parabolic dunes may initiate from blowout depositional lobes migrating downwind (e.g., Laporte-Fauret et al., 2022), or via vegetation colonisation along the margins of transverse dunes in transgressive dunefields (Hesp and Walker, 2013; Lopez and Hesp, 2023; Hesp, 2024). Parabolic dunes can also initiate on poorly vegetated foredunes, where vegetation is destructed by storms (e.g., Goff et al., 2009), human actions, fires, or grazing (Hesp and Walker, 2013).

The spatio-temporal evolution and geomorphological development of a parabolic dune is mainly regulated by sediment supply and vegetation growth (Hesp and Walker, 2023; Hesp, 2024). As a parabolic dune migrates downwind, sediment is lost to its trailing ridges. If the parabolic dune is not supplied with new sediment, vegetation establishment will dominate, eventually leading to the stabilization of the parabolic dune. When a parabolic dune is stabilizing, vegetation growth on the trailing ridges is often less compared to the still migrating depositional lobe. Consequently, the dune morphology may transform from U-shaped into V-shaped forms. This progression is illustrated in *Figure 4B*, where the more seaward parabolic dunes retain a U-shape, and the more landward parabolic dunes exhibit a V-shape.

2.2. Dune mobility and stability

Coastal ecosystems typically alternate between phases of mobility and stability (e.g., Arens et al., 2007; Gao et al., 2020; Provoost et al., 2011). Within a system, mobility and stability phases can also occur simultaneously (Arens et al., 2007). The most important driving forces that determine the phase of a coastal ecosystem are sand supply, wind energy and vegetation growth (e.g., Arens et al., 2007; Hesp, 2013; Gao et al., 2020). In general, high wind energy and sand

supply will result in mobility, while low wind energy and low sediment supply will result in stability. Because wind energy within a dune system generally is a relatively invariable force compared to sand supply and vegetation growth, the balance between dune mobility and stability comes down to the continuous contest between vegetation and sand, deciding which one takes the lead in shaping the dune landscape. While predominant aeolian sand dynamics will lead to dune mobility, predominant vegetation growth will lead to dune stabilization (Arens et al., 2013; Pye and Blott, 2017). Shifts between mobility and stability phases occur due to alterations in climate, sand distribution, or human influence (e.g., Arens et al., 2007; Gao et al., 2020; Provoost et al., 2011).

2.2.1. Trend towards dune stability

Historical observations reveal that from the 13th to 19th century, most European coastal areas were in a state of mobility (Provoost et al., 2011). The primary mobility drivers in this time period were the large-scale wood chopping (e.g., Arens et al., 2013) and grazing of domestic livestock (e.g., van der Maarel et al., 1985). The rabbit, introduced to Europe around 1150 AD, further intensified dune mobility by reducing vegetation succession (Provoost et al., 2011). Other human activities, including harvesting marram grass for domestic and agricultural purposes (e.g., Angus, 2001), also stimulated dune mobility.

Since the beginning of the 20th century, however, there has been a worldwide trend towards dune stabilization (e.g., Provoost et al., 2011; Gao et al., 2020). Based on Gao et al. (2020), dune stabilization factors can be categorized in four main drivers. The first stability driver is the change in land use. The removal of livestock from dunes to minimize aeolian dynamics, has promoted plant successions, resulting in an increase in tall scrubs and woodlands (e.g., van der Maarel et al., 1985). In addition, plant succession has been promoted by the decline in rabbit populations due to the Myxomatosis disease (e.g., Provoost et al., 2011; Sumption and Flowerdew, 1985). Within one year following the decline in rabbit population, an increase in vegetation growth was observed (Ranwell, 1960). The demographic expansion and industrial growth are also great causes for dune stabilization. Along many coastal areas an increase in infrastructure and urban housing projects has led to a loss of dune habitats (Gao et al., 2020). The second stabilization driver is climate change. Due to climate change induced temperature rise and rainfall, the growing season has been prolonged with approximately one month (Arens et al., 2013; Provoost et al., 2011). Additionally, vegetation growth is further stimulated by nitrogen input from air pollution (e.g., Arens et al., 2013). The third stabilization driver is the sediment decline by the construction of coastal and riverine constructions. Since fluvial sediments are a major source of sand for coastal ecosystems, the construction of river dams greatly reduced sand supply to coastal areas (e.g., Graffin et al., 2021). The fourth and likely most important stabilization driver is the anthropogenic coastal stabilization. In order to increase the volume and strengthen coastal foredunes, planting projects and sand-trapping fences were often applied (Gao et al., 2022). Sand-trapping fences have also been used to reduce sand drifting inland onto farms or infrastructure (e.g., Pelletier et al., 2009; Wendelken, 1974).

2.2.2. Mobility restoration projects

Recognizing the consequences of dune stabilization, nature and coastal managers nowadays believe that the restoration of dune mobility is important to restore biodiversity (e.g., Provoost et al., 2011; Hesp and Hilton, 2013) and to improve dune resilience to rising sea levels (e.g., Provoost 2011; Arens et al., 2013; Osswald et al, 2019). Currently, numerous dune mobility restoration projects are ongoing worldwide (e.g., Arens et al., 2004; Martínez et al. 2013; Arens et al., 2013; Hesp and Hilton, 2013). A widely applied restoration technique is beach nourishment, which involves adding sand to increase the width and sand volume of the beach (*Figure 5A,* e.g., Hanson et al., 2002; Elko et al., 2021). While large-scale beach nourishment can provide sediment for dunes to form, it takes a significant amount of time for dunes to develop, and additional nourishment is required due to wave induced erosion (Nordstrom & Jackson, 2013). Furthermore, the stabilized foredunes will still acts as a barrier preventing aeolian sand transport from the beach into the back dunes. Therefore, beach nourishment is a temporary solution that can be costly to maintain (Arens et al., 2013). There are also potential negative impacts on groundwater levels and ecological systems that are possibly related to sand suppletion (Schipper et al., 2021).

An increasing number of coastal restoration projects are incorporating the excavating of foredune notches (e.g., Ruessink et al., 2018; Laporte-Fauret et al., 2021), gaps in in the foredune that resemble natural trough blowouts (*Figure 5B*). Observations from foredune notching experiments along the coast of the Netherland (e.g., Ruessink et al., 2018; Arens et al., 2004) and other sites in western Europe (e.g., Laporte-Fauret et al., 2021) already concluded that foredune notches can act a sediment transfer system between beach and dunes and can be an effective channel for aeolian transport into the back dunes. Furthermore, the resulting bare sand patches allow for vegetation to rejuvenate to earlier stages of succession (Nordstrom, et al., 2007).

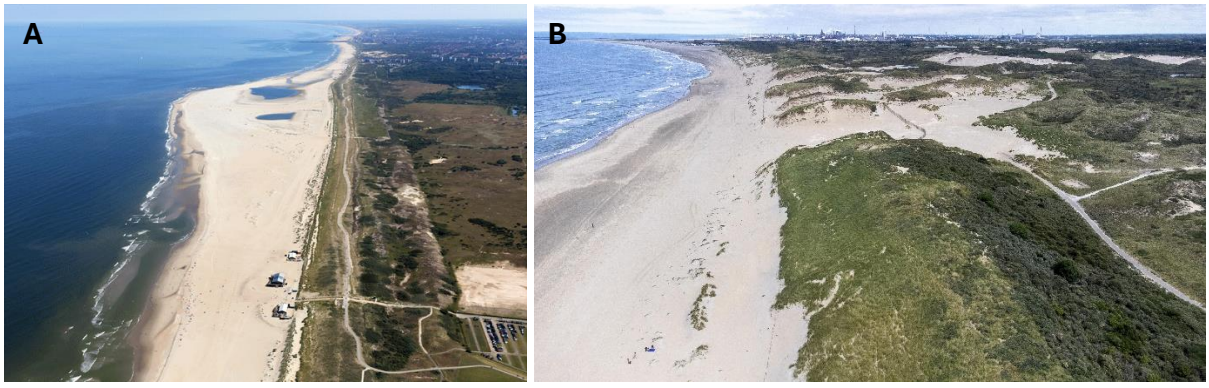

Figure 5. Aerial photographs of (A) "De Zandmotor" (sand motor), an experimental beach nourishment located along the Delfland coast, the Netherlands (Nolet and Riksen, 2019) and (B) excavated foredune notches along the Bloemendaal coast, the Netherlands (Rob van Wieringen, n.d.).

2.3. Aim and research questions

While the number of dune mobility restoration projects involving the excavation of foredune notches is increasing, in-depth knowledge on the physical-ecological relations that shape the evolution of these notches and associated depositional lobes is limited. Specifically, it remains unclear what drives the transitions between evolutionary phases, whether these transitions are

gradual or abrupt, and if there are thresholds or tipping points involved. This knowledge is crucial for understanding how long excavated foredune notches will stimulate aeolian dynamics into the back dunes and thus for how long notch systems will remain active. To properly investigate the evolutionary phase transitions described by Schwarz et al., (2019) (*Figure 3*), blowouts or foredune notch projects that have transitioned from the geomorphological to the ecological evolutionary phase need to be studied. Existing research on blowouts and excavated foredune notches, however, often covers only the first phase of the evolution (e.g., Pye and Blott, 2016; Ruessink et al., 2018). Although studies to blowouts at Island Beach (New Jersey) by Gares and Nordstrom (1995) and Padre Island (Texas) by van Kuik et al. (2022) and Jewell et al. (2017) observed a complete evolution, the physical-ecological relations shaping the evolution were not well studied.

The dunefield at middle Terschelling, where foredune notches were excavated in 1995, was selected as study site for this research, since vegetation has been recovering in large parts of the dunefield, indicating that the system is transitioning into the ecological stage. Additionally, the study area is located within the region of the Dutch coast wherefore freely available airborne lidar data is available. Both these factors make the restored dune field at middle Terschelling an ideal site to study the physical-ecological relations that shape the evolution of restored coastal dune ecosystems. Using areal data obtained from a Google Earth Engine (GEE; Gorelick et al. 2017) algorithm developed by van Kuik et al. (2022), specifically designed to compute the blowout sand surface area within a user defined region of interest, together with volumetric data obtained from the lidar surveys, this study aims to (1) quantify and analyse the temporal and spatial geomorphological evolution of a restored dune field at Terschelling and (2) explore whether the observed evolution is indicative of temporal changes in the feedback mechanisms between geomorphological processes and vegetation dynamics, including temporal changes in the strength of these interactions and thresholds or tipping points. Subsequently, the research questions of this study are:

1. What are the temporal and spatial changes in the blowout surface area of bare sand and blowout sand volume?
2. How are episodic, seasonal and gradual changes in blowout surface area reflected in temporal volumetric changes?
3. To what extent is the geomorphological evolution of the blowouts indicative of temporal changes in the feedback mechanisms between geomorphological processes and vegetation dynamics?

3. Study area

3.1. Location and climate

The study area is located on Terschelling, the second largest barrier island in the northern Netherlands. Terschelling has an elongated shape, stretching over 30 km from west-southwest to east-northeast. The northern, North Sea side of the island is a sandy coastline marked by 30 beach poles, or *rijksstrandpalen* (RSP) in Dutch, each spaced one kilometre apart. The dunefield at middle Terschelling, between RSP 15 and 20, is the study area of this research (*Figure 6*).

The climate on Terschelling is moderate maritime. Climate data for the study area are based on measurements by the Royal Netherlands Meteorological Institute (KNMI, 2024) at the Hoorn weather station, located approximately 4 km southwest of the study area. The 10-year average yearly temperature and precipitation are 10.6°C and 772 mm, respectively. Seasonal variations are significant, with average winter temperatures around 5°C and summer temperatures around 17°C. Precipitation is highest in autumn (85 mm) and lowest in spring (41 mm). Prevailing winds originate from westerly to south-westerly directions (*Figure 7*). Because the shore-normal direction at the study area is approximately 342°N (*Figure 6*), the prevailing wind directions are strongly onshore and offshore shore-oblique. Dominants wind directions in the months April to Novembre correspond with relatively weak oblique onshore winds, while the dominant wind directions in the months October to March correspond with relatively strong oblique offshore winds (Table 1). Because the Hoorn weather station is located on the southern side of Terschelling, approximately 4 km southwest of the study area, wind conditions may differ from those along the shore at the study area.

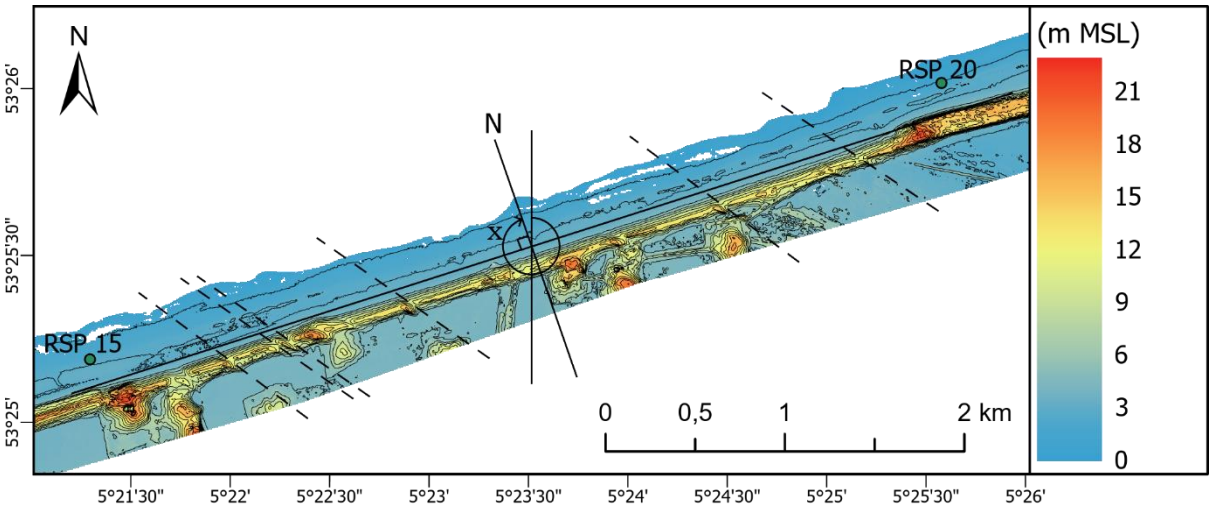

Figure 6. Elevation in de study area with respect to the Mean Sea Level (MSL), produced from the 1997 airborne lidar survey. Black contours have 1.5-meter interval. The green dots indicate the locations of the beach poles (RSP) between which the study area is located. The shore-normal (N) direction, indicated by x, at the study area is approximately 342°N. The approximate orientations of several excavated notches that were excavated in 1995 are indicated by black dotted lines.

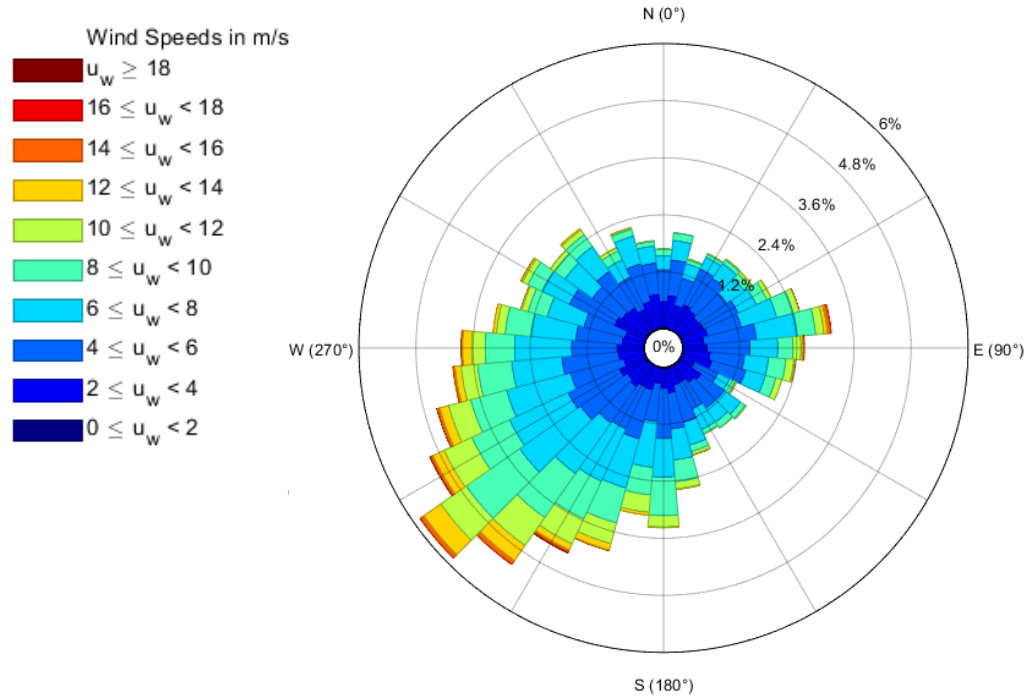

Figure 7. Wind direction-intensity histogram (wind rose) for the period 1995-2024, based on measurements at the Hoorn weather station by the Royal Netherlands Meteorological Institute (KNMI, 2024). The Hoorn weather station is located approximately 4 km southwest of the study area. The wind histogram was created using a MATLAB tool made by Daniel Pereira (2024).

Table 1. The dominant wind direction and average wind speeds and gusts based on observations between 04/2002 and 05/2024. The table was obtained from windfinder.com (Wind and Weather Statistic Terschelling Hoorn, n.d.).

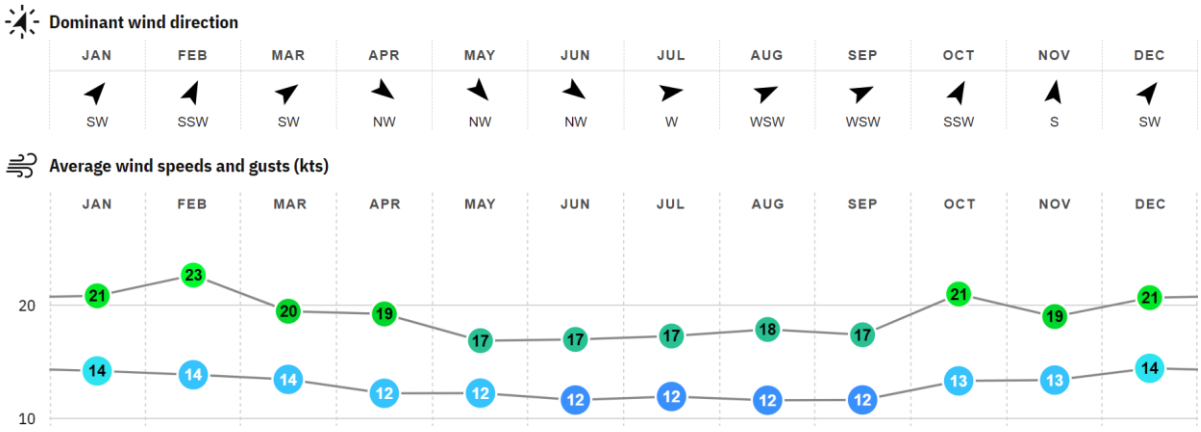

3.2. Foredune management and development

Before 1990, the Dutch coastline was primarily managed by using dunes as a buffer. Foredunes were extensively planted to capture as much drifting sand as possible, allowing the foredune to be eroded during severe storms (de Groen et al., 2019). However, several foredunes located in coastal areas that were experiencing severe coastal erosion were regularly shifted inland in order to minimize coastal erosion (Quataert et al., 2020).

The coastline at Middle Terschelling, between RSP 15-20, was one of the coastlines experiencing severe coastal erosion (e.g., Noordstra, 1991; van der Wal, 1996; Arens et al., 2007; POK, 1998). To minimize erosion, the foredune was gradually shifted inland from the 1960s to the early 1990s, creating a so called “rolling foredune” (van der Wal, 1996). The rolling foredune resembled an unvegetated sand dune were aeolian sand transport over the rolling foredune was trapped by windbreaks made of reeds and willow branches that were placed on the dune crest, as well as marram grass that was planted at the inner toe (*Figure 8A*; van der Wal, 1996). Occasionally, bulldozers were used to remove vegetation from the seaward side of the foredune, stimulating sand transport onto the foredune (e.g., van der Wal, 1996; Arens et al., 2007).

The management efforts resulted in a high, narrow and straight "sand dike" that prevented almost all sand aeolian transport towards the hinterland (e.g., Coumou and Cleveringa, 2020). In combination with increased nitrogen deposition, lower groundwater levels, reduced grazing and accelerated plant succession, the presence of rare species in the dunefield greatly reduced (Löffler et al., 2008). Despite all management efforts, the coastline retreated 100 to 200 m inland from 1965 to 1990 (*Figure 8B*; Noordstra, 1991). More images of the rolling foredune can be found in Appendix 1.

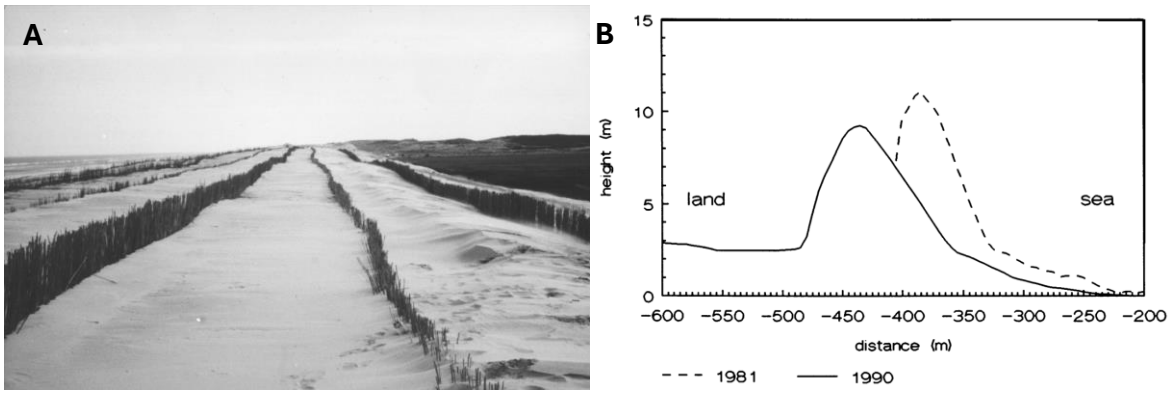

Figure 8. (A) Image of the rolling foredune (at an unknown date) on Terschelling between RSP 15 and 20 and (B) a schematic cross section of the rolling foredune development between 1981 and 1990 at RSP 17 (van der Wal, 1996).

In 1990, the government and parliament of the Netherlands introduced a new coastal defence policy named “dynamic maintenance” (e.g., van der Wal, 1996; Hillen and Roelse, 1997; POK, 1998; Arens et al., 2007). The policy aims to sustainably protect against coastal erosion and, where possible, provide more space for natural processes in coastal dunes. The new policy also states that the entire coastline has to be maintained at its 1990 position.

As part of the dynamic coastal defence policy, a shoreface suppletion of 2.1×10^6 m^3 sand was conducted in 1993, between RSP 13.7 and 18.1, depositing 455 m^3/m sand (Arens et al., 2007). Furthermore, the maintenance of the rolling foredune was abandoned. Instead, dune dynamics were stimulated by removing the existing windbreaks and branches, allowing drifting sand to transport over the foredune. Additionally, notches were excavated through the foredune (e.g., Arens et al., 2007; Coumou and Cleveringa, 2020). Taking the dominant wind direction into account, the notches were excavated diagonally through the foredune, in northwest to southeast direction (*Figure 6*), allowing the wind to funnel drifting sand through the notches. Until 2003,

vegetation emerging seaward of the notches was removed to stimulate the landward transport of sand. After 2003, stimulating intervention were not necessary anymore, and the only interventions were a notch relocation at RSP 19.1 to 19.4 and the placement of windbreaks (at unknown locations) to prevent sand drifting onto an adjacent pasture (Arens et al., 2007). Except for 1993, sand nourishments were not conducted because the coastline has been expanding since the implementation of the dynamic restoration measures (Coumou and Cleveringa, 2020).

Due to sand drifting beyond the position of the rolling foredune into the back dunes (*Figure 9*), vegetation has rejuvenated, and various habitats have emerged in the new valleys, vegetated and unvegetated dunes. Species adapted to dry conditions established themselves on the thickly drifted sand layers, whereas species favouring calcareous conditions appeared in the moist areas (Coumou and Cleveringa, 2020).

Figure 9. Areal images of sand drift at middle Terschelling between RSP 15 and 20 in the year 1998. Images from: 't Behouden Huys (POK, 1998).

4. Methodology

4.1. Data collection

4.1.1. Lidar data

Lidar data was used to quantify and visualize temporal and spatial volumetric changes within the study area. Lidar is a remote sensing method that uses pulsating laser light to determine distances between the laser source and a surface (Popescu, 2011). A lidar survey generates a collection of points in three-dimensional space, also known as a point cloud. Due to its high accuracy and three-dimensional data collection, lidar is commonly used for geospatial mapping. To obtain topographic data of the Dutch coastal zone, airborne lidar surveys have been conducted annually by the Dutch governmental organisation Rijkswaterstaat since 1996 (Bechev-Van der Burgh et al., 2011). The collected data is available through Utrecht University servers, where each year's data is segmented over multiple sections and stored as raw (from 2005 onwards) or processes (prior to 2005) point cloud data. Data for the years 1996, 2001, 2003, 2005 and 2020 either did not fully cover the study area or was not available through the Utrecht University servers and was therefore not incorporated in the dataset. Consequently, the earliest available data included in the dataset was from the 1997 survey.

4.1.2. Satellite imagery

To quantify and visualize temporal and spatial development of the vegetation and sand surface area within the study area, a Google Earth Engine algorithm developed by van Kuik et al. (2022) was utilized. This algorithm was developed specifically to compute time series of blowout sand surface areas within a region of interest (ROI) using Landsat and Sentinel-2 satellite imagery. Besides the already incorporated Landsat-4, -5, -7, -8 (30×30 m) and Sentinel-2A, -2B (10×10 m) collections, the Landsat-9 (30×30m) collection was integrated in the algorithm. The same Tasselled Cap Transformation for the Landsat-8 collection was also used for the Landsat-9 collection (Tasselled Cap Transformation for Landsat 8 and 9, 2023). Due to clouds or shadows created by clouds and topography, not all images were usable. The algorithm therefore filtered and removed images had a cloud cover below 10% within the ROI. Images were also ensured to have 100% ROI coverage. Due to failure of the scan-line-corrector of the Landsat-7 sensor, the minimum Landsat-7 ROI coverage was set to 70%. The algorithm filled the failed scan lines using Landsat-5 or -7 images at nearby dates.

4.2. Data analysis

4.2.1. Volume change

To ensure compatibility and comparability of the data, it was crucial to standardize the formatting, projection and spatial resolution of the data. Standardizing was performed using the ArcGIS Pro desktop GIS software application (ESRI, 2024). As the study area was segmented and stored over multiple sections, each year's elevation files had to be merged into one. Data stored as raster files were merged using the *Mosaic To New Raster* tool. Several raster files contained cells with unavailable information within the study area. These cells were filled using the *Nibble* tool, which assigned the value of the nearest neighbour to the empty cells. Using the nearest neighbour to replace the value of an existing cell is effective for nearby distances. However, as the distances increase, the connection weakens, and the results become less reliable. Since

most missing cells were isolated or part of small clusters, the filled values in the output raster are expected to be reasonable. The *Raster Calculator* tool was utilized to convert the units from centimetres to meters. To merge data stored as point cloud files, the *lasmerge* tool (LAStools, 2024) was used. Using the *LAS Dataset To Raster* tool, the merged point clouds were then transform to raster files using binning interpolation. Raster cells that did not contain points were determined using linear triangulation interpolation. Since raster files prior to 2005 had a spatial resolution of 5×5 m, the spatial resolution of the rasters created from point clouds was set to 5×5 m as well. Furthermore, the extent of the rasters was adjusted to match the cell alignment of the previously merged rasters, and the output coordinate system was set to the default coordinate system, A*mersfoort_RD_New*. To identify changes in elevation over time, annual elevation difference models were created by subtracting each year's elevation raster from its succeeding year's elevation raster.

Based on the 1997 elevation model, the study area was divided into three sections, the rolling foredune, beach and hinterland (*Figure 10*). The beach-foredune transition was based on the +3 m MSL elevation contour, which is generally used as the foredune foot height in the Netherlands (e.g. Stuyfzand et al., 2010; de Groen et al., 2019; Quataert et al., 2020). The landward boundary of the rolling foredune was also determined based on the +3 meter elevation contour, supported by satellite imagery from 1997. The beach section was defined by as the area seaward of the rolling foredune, ranging from +1 to +3 m MSL. Elevations below +1 m were excluded from the region to minimize the influence of tides, while still covering a large portion of the beach. The hinterland section was defined as the area between the landward edge of rolling foredune and the boundary of the elevation files, excluding areas that did not belong to the dunefield such as agricultural lands. The study area boundaries do not match exactly with the locations of RSP 15 and 20 (*Figure 10*). The cross- and alongshore dimensions of the study area are 4976 by 290-550 m, respectively.

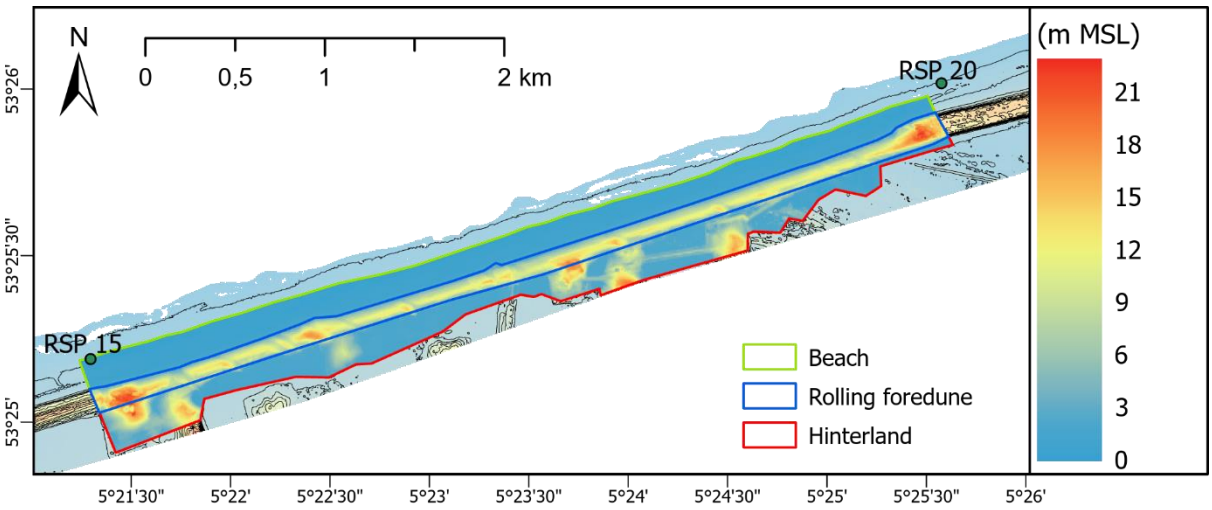

Figure 10. The rolling foredune, hinterland and beach section, displayed on the 1997 elevation model. The seaward edge of the beach section is based on the +1 meter MSL and the landward edge of the hinterland section is based on the lidar survey boundary, excluding agricultural lands. The cross-shore boundaries do not match exactly with the locations of RSP 15 and 20. Therefore, the alongshore dimension of the study area is 4976 m. The cross-shore dimension ranges from 290 to 550 m.

For volumetric computations it was necessary to collect the data of all raster cells per section per year. The workflow that was used to collect this data is illustrated in *Figure 11*. First, a unique value had to be assigned to each raster cell. A raster, where each cell is assigned a unique value, or ObjectID (OID), that matched the edges of the raster cells was made using the *Fishnet* tool (*A*). The *Zonal Statistics as Table* tool was then used to assign all raster cell values to the corresponding overlaying OID's (*B*). The OID's within the thee sections were detected using the *Spatial Join* tool (*B*). With this step, the OID's within a section are assigned the Join Count 1, and OID's outside of the area are assigned the Join Count 0 (*C*). The OID's with Join Count 1 were then linked to the corresponding elevation values using the VLOOKUP function in Excel (*D*). The output of this function are the raster cells per section (*E*). These steps were repeated for all three sections for each year's raster file.

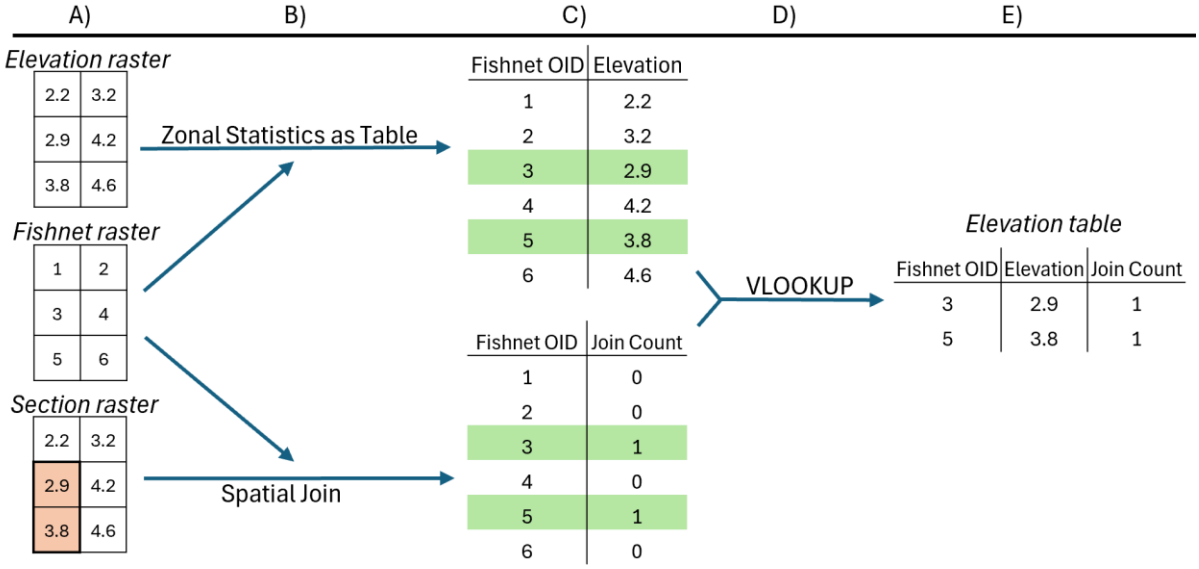

Figure 11. Diagram of the workflow used to collect raster data within a section using the Zonal Statistics at Table and Spatial Join tools (B) in combination with the VLOOKUP function (D). The orange highlighted cells (A) represent a section raster, and the green highlighted cells (C) represent the section cells that are looked up and linked together based on their OID. The workflow is utilized to obtain the elevation table for each section for each year's raster zonal statistics table (E). The values used in the diagram are for illustrative purposes and are not based on true elevation data.

Using each year's elevation raster data per section, the total sand volume and annual sand volume change were calculated for the three sections separately and combined. The total sand volume over time was calculated by subtracting the 1997 cell data from all other year's corresponding cell data. To calculate the annual sand volume change, each year's cell data was subtracted from each year's preceding corresponding cell data. Due to missing elevation data for several years, some volume changes are biennial instead of annual. To obtain a complete annual timeline, the biennial volumes changes were divided by two, and to account for the raster cell size of 5×5 m and obtain volume changes in cubic metres (m^3), volumes were multiplied by 25. Additionally, annual volume changes were divided by the alongshore length of the study area (4976 m). In addition to volume and annual volume change, the absolute sand volume and absolute volume change were calculated by using the absolute value of the elevation change cell values.

4.2.2. Areal changes and vegetation establishment

Sand surface areas within the filtered Landsat and Sentinel collection were obtained using the algorithm by van Kuik et al. (2022). A concise overview of the algorithm workflow is provided below. For a more detailed explanation on the workflow steps, see van Kuik et al. (2022).

(1) Using the spectral indices Normalized Difference Water Index (NDWI) and Normalized Difference Vegetation Index (NDVI) alongside Otsu thresholding, the initial estimated locations of water, sand, and vegetation pixels within each image were identified. NDWI histograms were used to distinguish water and land, while NDVI histograms were used to distinguish land and vegetation.

(2) In order to apply linear spectral unmixing (LSU), pixels with homogeneous land covers (image endmembers) had to be identified. It was assumed that the most frequent index values of the initial estimates represent the image endmembers. Endmembers were therefore determined as pixels around local maxima inside the NDWI or NDVI histogram, with a buffer of 5% on both sides. LSU was then used to estimate fractional abundances of sand, vegetation, and water within every pixel.

(3) To quantify the sand surface area within the collected images, a Blowout Region of Interest (BROI) had to be defined within the ROI. The BROI used for this study was similar to the area of both the rolling foredune and the hinterland section (*Figure 10*). Pixels within the BROI that were identified as water were reclassified as sand. For al collected images, the blowout sand surface area within the BROI was computed by multiplying the number of pixels with a fractional sand cover exceeding 50% (f_c>50%) by the pixel area.

To assess the relationship between vegetation establishment and dune elevation, erosion, and deposition, cross-shore profiles were created. To investigate the differences between vegetated and unvegetated areas, profiles were created along areas that have experienced vegetation regrowth, as well as areas that have remained unvegetated. When the fractional sand cover was below 50% (f_c<50%) and the pixel was not classified as sand, the pixel was assumed to be a vegetated pixel with a fractional vegetation cover above 50% (f_c>50%). Elevation data along the profiles was collected using the ArcGIS *Stack Profile* tool.

5. Results

5.1. Sand volume changes

5.1.1. Quantified volume changes

The sand volume in total study area, equal to the beach, rolling foredune and hinterland sections combined, gained ~15.8×10^5 m^3 (0.6×10^5 m^3/yr) over the entire study period (*Figure 12A*). Given the study area width of 4976 m, the average sediment input into the study area was ~12.2 m^3/m/yr. While over the entire study period the sand volume in the beach and hinterland sections increased with ~9.6×10^5 and ~11,9×10^5 m^3, respectively, the sand volume in the rolling foredune section decreased with ~5.7×10^5 m^3. The R-squared of the total area and beach section linear regression models (R^2=0.952 and R^2=0.944, respectively) suggest that the sand volume in these areas increased linearly. The sand volume in the hinterland and rolling foredune sections experienced a more stagnating trend.

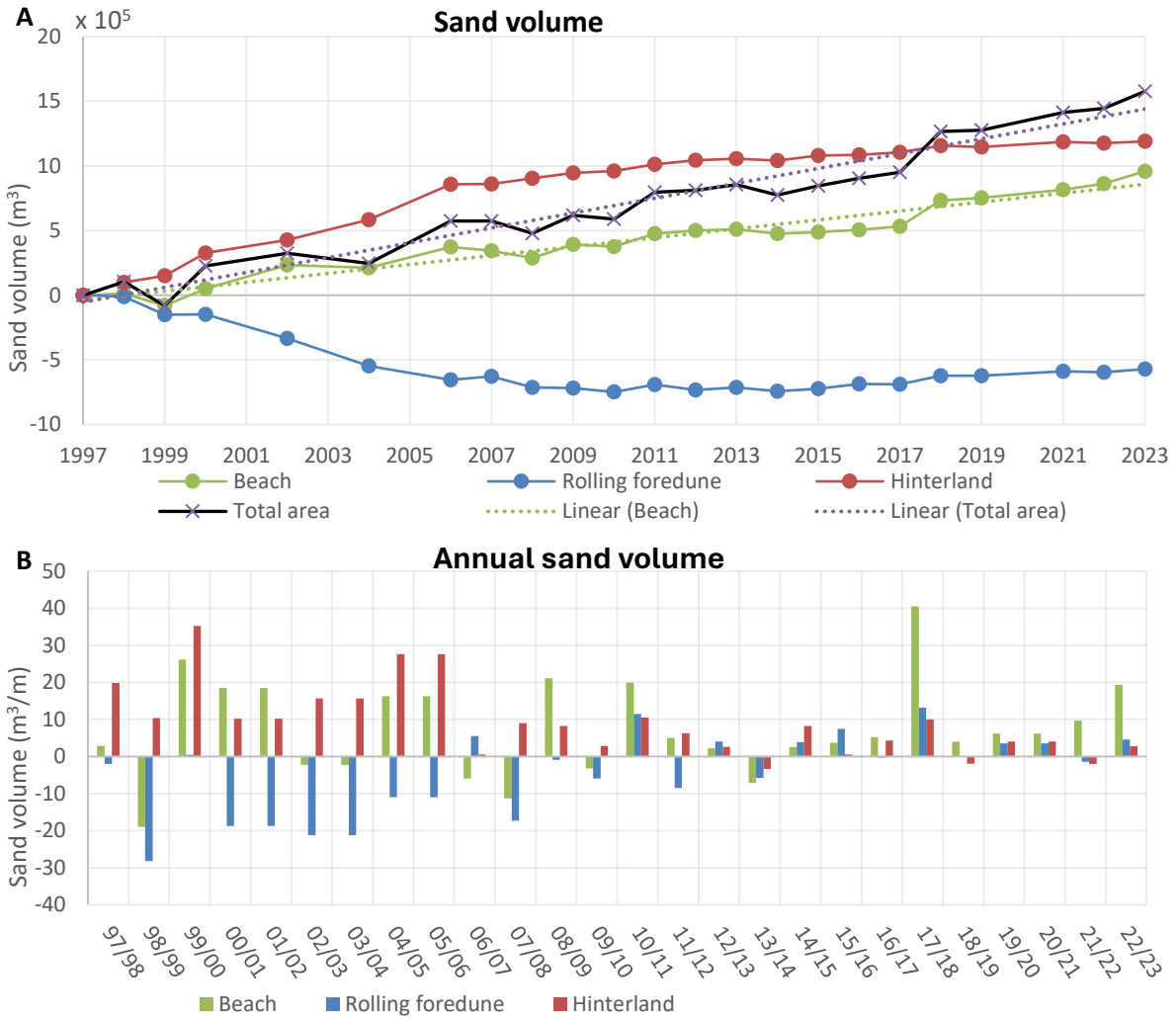

Figure 12. (A) The sand volume in the beach, rolling foredune and hinterland sections separately and combined, during the period from 1997 to 2023, taking 1997 as reference year. The purple and green dotted lines are the best-fit linear regression models for the total area and beach section (R^2=0.952 and R^2=0.944, respectively). (B) The annual sand volume changes in the sections are divided by the alongshore length of the study area (4976 m). Due to missing elevation data for several years, volume changes for 2000-2002, 2002-2004, 2004-2006 and 2019-2021 are biennial instead of annual. To obtain a complete annual timeline, the biennial volumes changes are divided by two.

While the rolling foredune section lost sand volume rapidly from 1997 to 2006 (~72.8×10^3 m^3/yr), the hinterland and beach sections gained sand volume rapidly (~95.3×10^3 and ~41.4×10^3 m^3/yr, respectively). Since 2006, the sand volume in the rolling foredune section remained more or less constant. However, from 2014 onwards, the rolling foredune section started gaining sand volume slowly (~6.5×10^3 m^3/yr). The beach and hinterland sections slowly gained sand volume from 2006 onwards. However, while the hinterland section sand volume gain from 2006 to 2023 was relatively constant (~19.6×10^3 m^3/yr), the beach section started to gain volume more rapidly from 2017 onwards (~71.0×10^3 m^3/yr). Especially between 2017 and 2018 the sand volume gain in the beach section was notably large (~2.0×10^5 m^3). The highest total annual sand volume change (63.6 m^3/m) was also observed between 2017 and 2018 (*Figure 12B*). Overall, the period 1997-2006 is characterized by rapid sand volume changes, 2006-2017 by stable or slowly gaining sand volumes, and 2017-2023 by slowly gaining sand volumes in the rolling foredune and hinterland sections and a more rapid sand volume gain in the beach section.

The total absolute sand volume change in the total study area was ~10.4×10^6 m^3 (*Figure 13A*). While the R-squared of the beach section linear regression model (R^2= 0.998) suggests that the absolute sand volume in the beach section has been constant over time, the hinterland and rolling foredune sections, as well as the total area, experienced a more stagnating trend (*Figure 13A and B*). The stagnating trend indicates that the dynamism in the hinterland and rolling foredune sections, as well as in the total area, declined over time. Between 2017-2018 and 2021-2023, the dynamism in the beach section was higher than the other two sections (*Figure 13B*). The annual absolute sand volume ranges from 143.3 m^3/m (7.1×10^5 m^3) between 1999-2000 to 49.5×10^5 m^3/m (2.5×10^5 m^3) between 2019-2020 and 2020-2021 (*Figure 13B*). While the total absolute sand volume in the rolling foredune section was ~46.9×10^5 m^3, the total absolute sand volume in the beach and hinterland sections were ~28.9×10^5 and ~27.9×10^5 m^3, respectively (*Figure 13A*). This indicates that dynamism has been greatest in the rolling foredune section. While from 1997 to 2023 the volume change within the rolling foredune section was lower compared to the other sections (*Figure 12A*), the dynamism in the rolling foredune section was higher (*Figure 13A*).

5.1.2. Spatial volume changes

Elevation and elevation difference models (Appendix 2, 3) reveal the development of geomorphological features. The 1997 elevation model reveals the location of the excavated foredune notches, visible as depressions orientated diagonally through the foredune. Over the years, the foredune migrated landward, the excavated notches became less distinct, the beach became progressively higher, and sand deposition seaward of the rolling foredune gradually formed a new foredune. In 2004 this new foredune reached elevations higher than 5 m MSL. On the western part of the beach, seaward of the new foredune, the growth of embryo dunes is visible since 2018. By 2023, several embryo dunes reached elevations higher than 5 m MSL. While erosion and deposition initially occurred along most of the dunefield stretch, it occurs only at several specific areas during the last few years. Erosion of the rolling foredune, formation of new foredunes and transgressive sand sheets, and growth of embryo dunes on the beach can also be observed in the 1997-2023 elevation difference model (*Figure 14*).

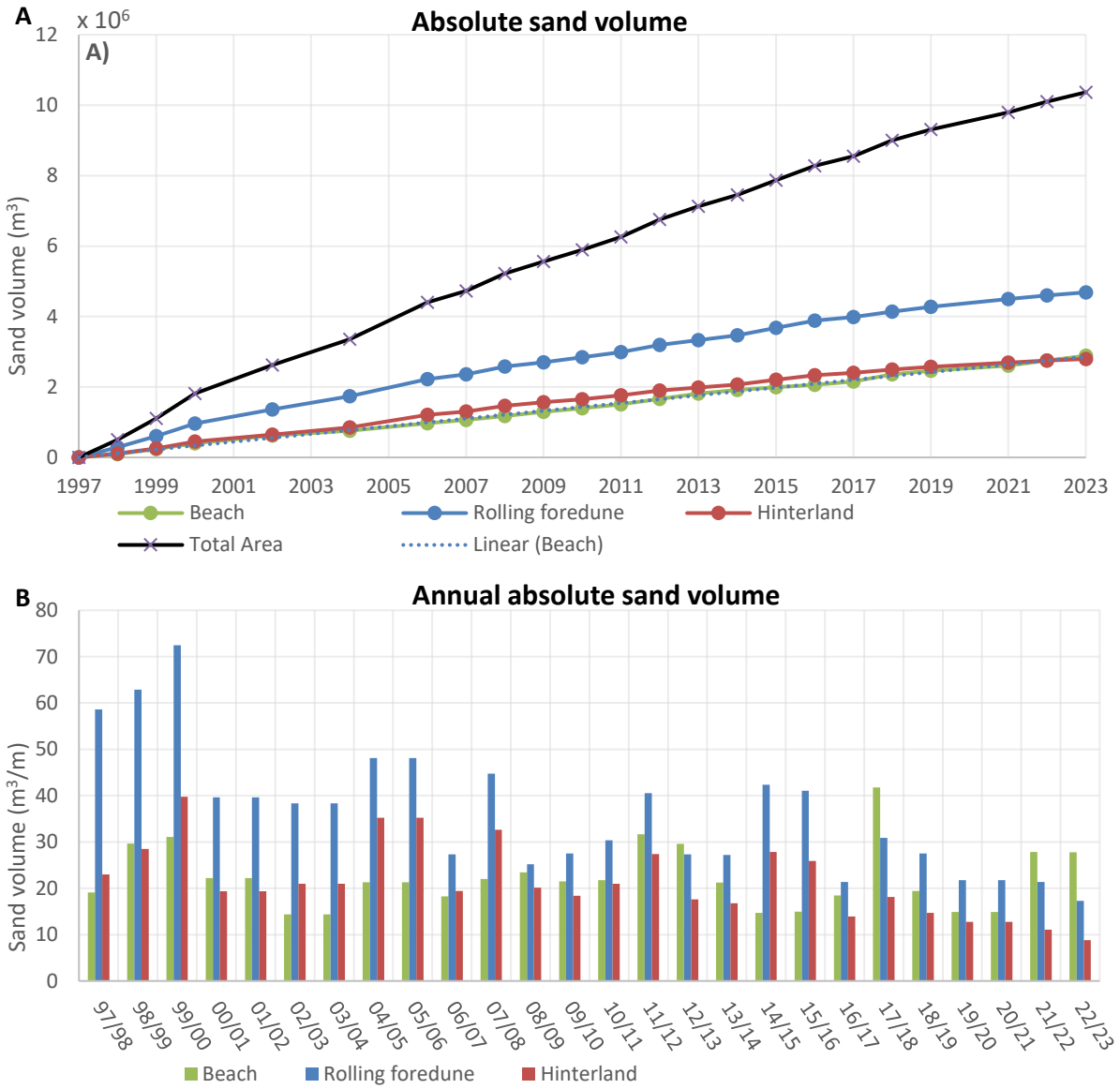

Figure 13. (A) The absolute sand volume change in the beach, rolling foredune and hinterland sections separately and combined, during the period from 1997 to 2023, taking 1997 as reference year. The dotted line is the best-fit linear regression model (R^2=0.998) for the beach section. (B) The annual absolute volume change in the sections divided by the alongshore length of the study area (4976 m). Due to missing elevation data for several years, volume changes for 2000-2002, 2002-2004, 2004-2006 and 2019-2021 are biennial instead of annual. To obtain a complete annual timeline, the biennial volumes changes were divided by two.

Elevation difference models were also created for the time intervals that were observed in the sand volume development (*Figure 12A*), where 1997-2006 is characterized by rapid sand volume changes, 2006-2017 by stable or slowly gaining sand volumes, and 2017-2023 by slowly gaining sand volumes in the rolling foredune and hinterland sections and a more rapid sand volume gain in the beach section. From 1997 to 2006, while large areas of the rolling foredune experienced erosion, deposition occurred in the hinterland section, adjacent to the rolling foredune, and along the northern border of the rolling foredune (*Figure 14*). This pattern of erosion and deposition occurred along the entire foredune stretch, except for the parking lot, located at roughly 5°23'20", and the eastern and western part of the foredune. Between 2006 and 2017, large areas along the border of the rolling foredune and hinterland section eroded. Deposition occurred in the

hinterland, adjacent to the eroding areas, indicating the further migration of sand in landward direction, and along the northern border of the rolling foredune. From 2017 to 2023, the migration of several lobes within the dunefield can be seen through the erosion and adjacent landward deposition. Additionally, deposition occurred along the eastern part of the southern border of the beach section, and in the western part of the beach section.

The elevation difference models reveal that the apparent volumetric stabilization in the rolling foredune and hinterland sections since 2006 (*Figure 12*) is largely the result of both sand deposition and erosion within the sections cancelling each other out. Therefore, the volumetric stabilization within the sections does not mean that dynamism ceased.

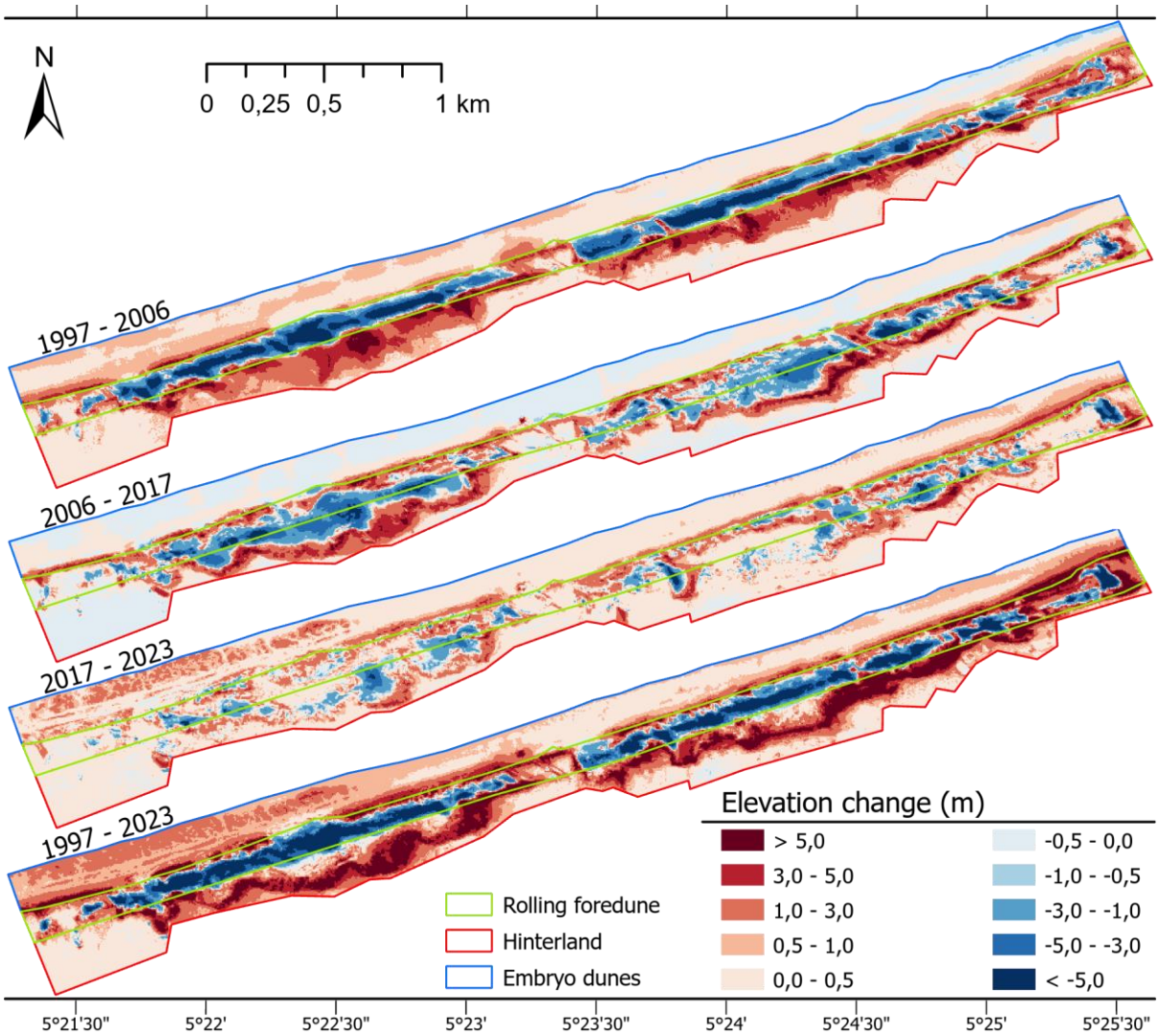

Figure 14. Elevation difference models for the whole study period (1997-2023), as well as for the periods 1997-2006, 2006-2016 and 2016-2023, where red colours indicate an increase in elevation (deposition) and blue colours indicate a decrease in elevation (erosion).

5.2. Sand area changes

5.2.1. NDVI Otsu thresholding

The time series of the computed sand surface areas (*Figure 15*) reveals a curve with seasonality and many outliers. The outliers are the result of cloud cover over vegetation being identified as sand, cloud cover over sand not being identified as sand, failed Landsat-7 scan line fill, incorrect geolocation of images, or a combination of the above. Ignoring outliers, the time series initially appears to be a consistent pattern with seasonality. However, the seasonality does not match the expectations. Typically, higher sand surface areas are anticipated in autumn and winter due to reduced vegetation growth and cover, and lower sand areas in spring and summer due to increased vegetation growth and cover, similar to sand surface area developments produced by Van Kuik et al. (2022). The observer seasonality, however, is reversed. The reversed seasonal pattern is particularly evident in the data points from 2015 onwards.

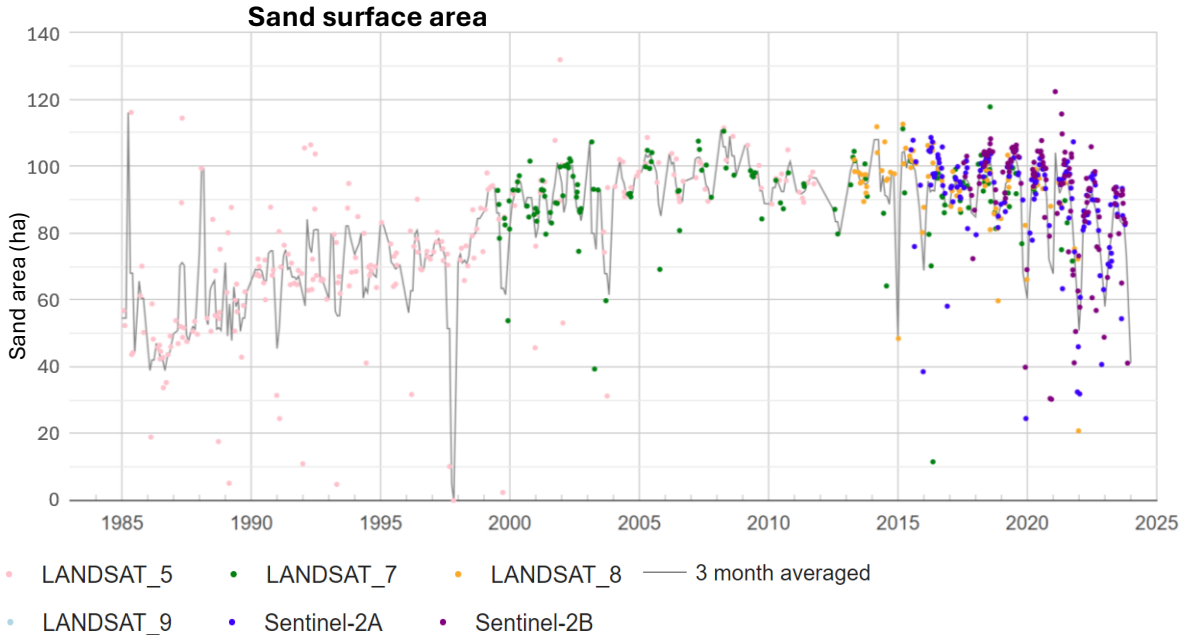

Figure 15. Time series of the sand surface area (ha) within the BROI (the area equal to the rolling foredune and hinterland section) for all collected satellite images between 1985 to 2024. The black line represents the 3-month averaged sand surface area.

The reversed seasonality is likely related to the application of the Otsu's thresholding method, which assumes that the NDVI histogram of the images contains two classes of pixels (vegetation and sand), forming a bi-modal histogram. However, the lower NDVI reflectance in autumn and winter compared spring and summer causes sand and vegetation peaks within the histogram to be closer together (*Figure 16*). Consequently, in spring and summer, the Otsu threshold is much higher compared to the autumn and winter Otsu threshold, leading to more vegetation being identified as sand in spring and summer compared to autumn and winter, leading to the reversed observed seasonal pattern in the computed sand surface areas. The Otsu computed from the NDVI histograms of the collected images (*Figure 17*) confirms the seasonality in the Otsu thresholds. It is visible that the Otsu threshold is at its lowest around the turn of the year, and peaks in the summer months.

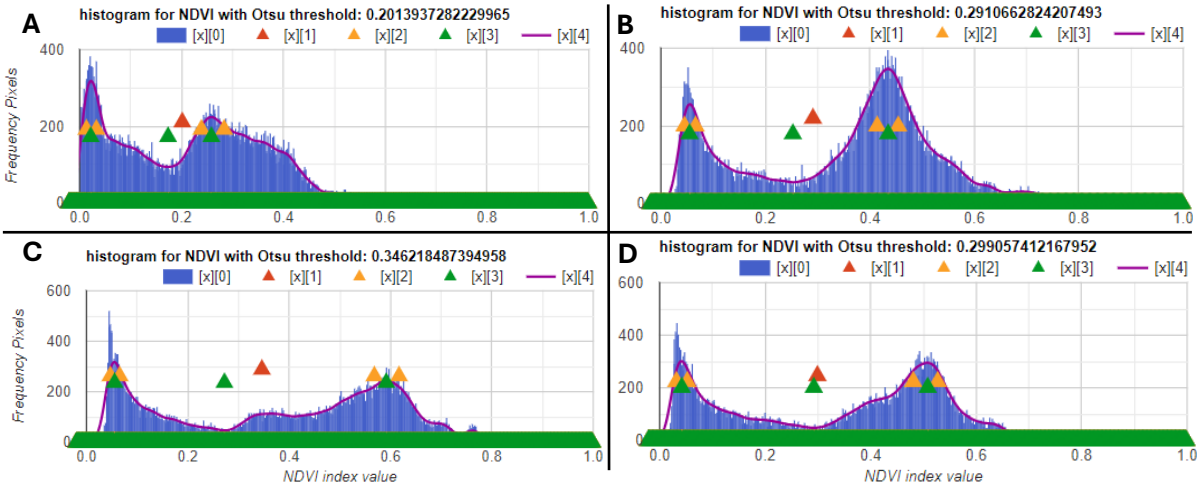

Figure 16. Examples of NDVI histograms and NDVI Otsu thresholds (red triangles) at collected images from (A) 2018-01-08, (B) 2018-05-08, (C) 2018-08-31 and (D) 2018-10-10.

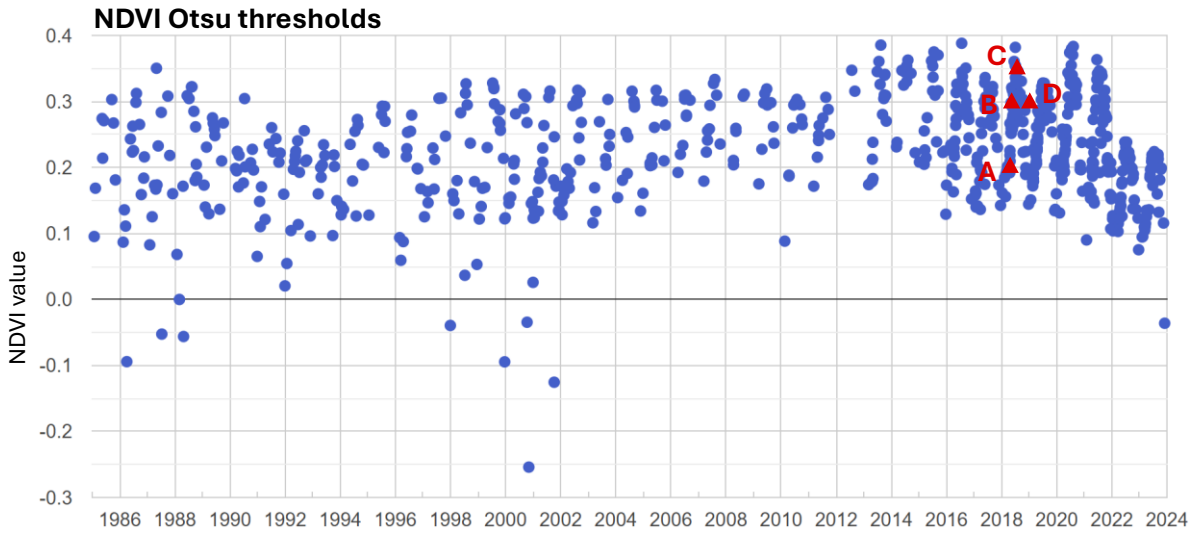

Figure 17. Time series of the NDVI Otsu thresholds computed from the NDVI endmember histograms of the collected images (Figure 15). The red triangles indicate the NDVI Otsu thresholds at collected images from (A) 2018-01-08, (B) 2018-05-08, (C) 2018-08-31 and (D) 2018-10-10.

An example of the sand surface geometry for 23 April 2018 is displayed in *Figure 18*. The section of the sand surface geometries within A1 for the dates of which the NDVI histograms are displayed in *Figure 16*, are presented in *Figure 19*. The geometry from January (A) had the lowest Otsu threshold (~0.2). Due to many topographic shadows resulting from a low sun angle, the sand surface area appears to be underestimated. The geometry from August (C) had the highest Otsu threshold (~0.35), and the sand surface area appears to be overestimated. The geometries from May (B) and Octobre (D) had similar Otsu thresholds (~0.3). Similar to January, the October image had many topographical shadows. Taking the sun angle, Otsu threshold and availability of imagery into account, it was decided to filter images from March, April and May, and to forego the seasonal analysis.

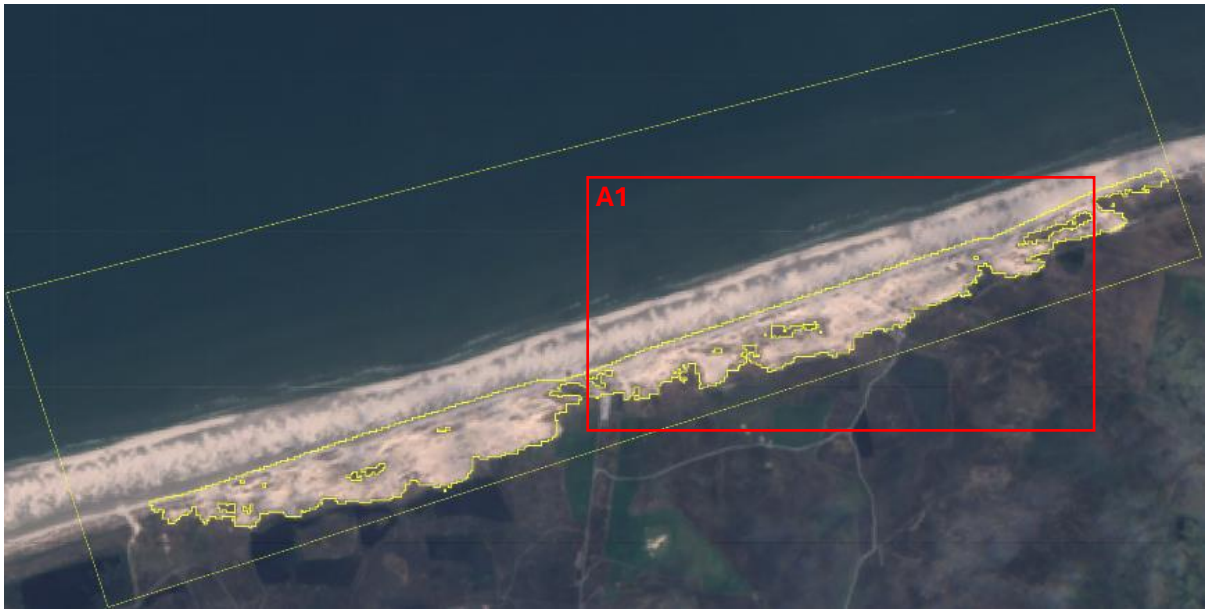

Figure 181. The sand surface area geometry (yellow polygon) for 23 April 2018 (Sentinel-2B), with a surface area of 1.035.256 m^2. Sand surface area geometries within section A1 are displayed in Figure 19.

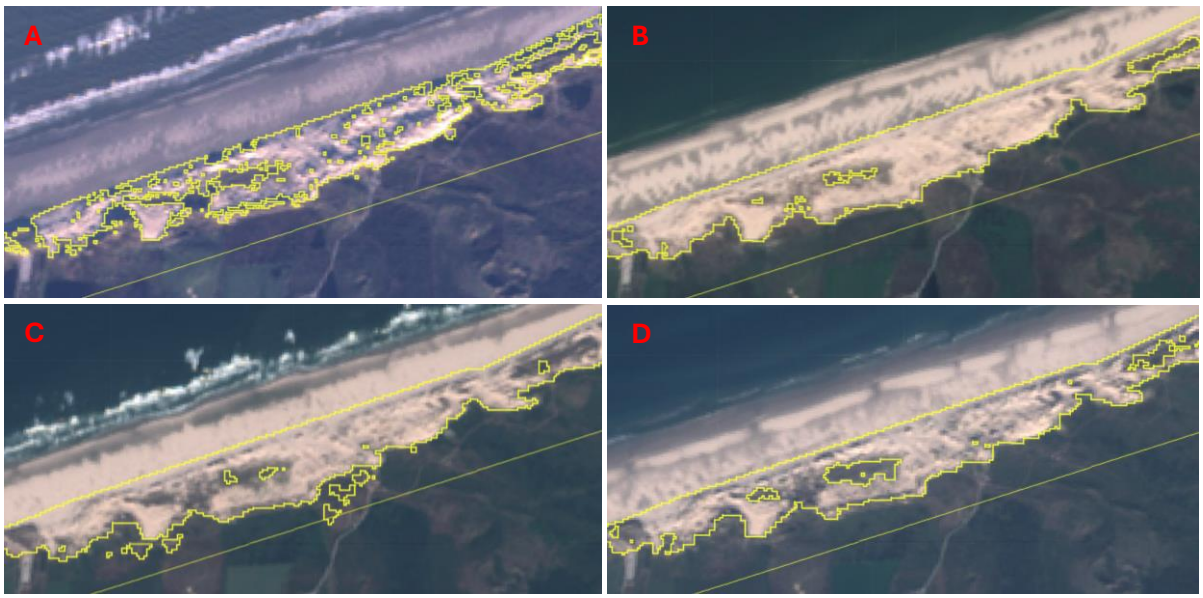

Figure 19. Sand surface geometries within to section A1 (Figure 18) at (A) 2018-01-08, (B) 2018-05-08, (C) 2018-08-31 and (D) 2018-10-10.

Despite filtering on March, April and May, sand surface area data points were widely scattered (*Figure 20*). However, trends can still provide valuable data. Prior to the implementation of the restoration measures in 1995, an increase in sand surface area is observed. This increase is the result of the gradual landward migration of the rolling foredune, rather than the formation of blowouts. Since the foredune was managed as a dynamic system from 1995 onwards, sand transported landward, leading to an increase in the sand surface area. However, around 2005, the sand surface area began to stabilize, and since approximately 2016, it has started to decrease. The R-squared values of the linear regression models for the specified time periods are 0.87 (1985-2004), 0.007 (2005-2015), and 0.43 (2016-2023). The corresponding slopes of the time periods are approximately 2.85 ha/yr, -0.15 ha/yr, and -2.23 ha/yr, respectively. Based on the

linear regressions, the sand surface area increased ~25.6 ha from 1995 to 2004. From 2016 to 2023, the sand surface area decreased ~13.4 ha. The sand surface area in 2023 had returned to a level similar to that of 1999. If the current trend continues, the sand surface area is projected to reach its 1995 value around 2028.

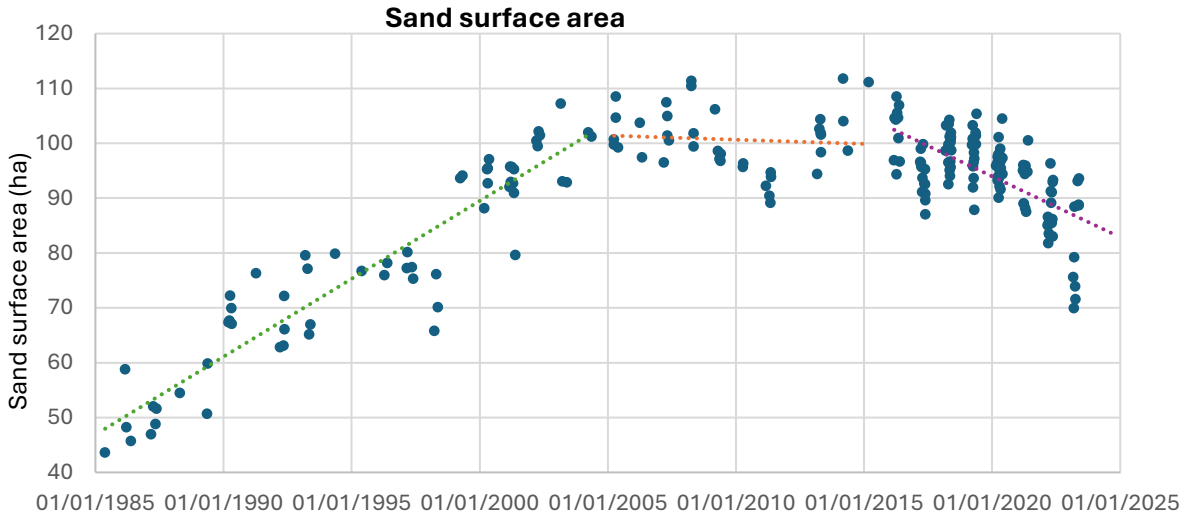

Figure 20. Time series of the sand surface area in the BROI (the area equal to the rolling foredune and hinterland section combined) filtered for the months May, April and March. The green, orange and purple dotted lines represent the linear regression models for the periods 1985-2004 (R^2=0.87), 2005-2015 (R^2=0.007) and 2016-2023 (R^2=0.43), respectively.

5.2.2. Sand surface areas and vegetation establishment

Sand surface area geometries from April were selected to determine the locations where vegetation (f_c>50%) has re-established. If no image for April was available, an image from March or May was used (Appendix 4). Based on trends observed in the sand surface area time series (*Figure 20*), several sand surface area geometries during the increasing or stable (1997-2015) and decreasing (2016-2023) periods are presented in *Figure 21A and B,* respectively. Most sand drift occurred at the middle section of the foredune (S1-2), forming alongshore sand sheets. Similar to volumetric changes (*Figure 14*), sand drift was limited at the parking lot (P), as well as the western and eastern sections of the foredune (A1-2). Vegetation re-establishment caused the sand surface area to decrease over time. This occurred mainly along the edges of the sand sheets and in box B1-3 (*Figure 21B*).

Five cross-section profiles were created to analyse the evolutionary path of the dunefield and to determine the relation between vegetation establishment (f_c>50%), elevation and dynamism. Profiles C1-C'1, C2-C'2 and C4-C'4 go through areas where vegetation has re-established (*Figure 22*). All three profiles show the landward migration of the rolling foredune from 1997 onward, resembling a transgressive sand sheet. While at profiles C1-C'1 and C4-C'4 the new foredunes formed seaward of the rolling foredune position from 1997 onwards, the new foredune at profile C2-C'2 formed around 2009, at the position of the rolling foredune. Deflation basins formed between the new foredunes and the landward migrating sand sheets. Over time, the deflation basins decreased in elevation, reaching elevations around 2.5-3 m MSL between 2013 and 2017. Once those elevation were reached, the basin started to gain elevation slowly (max. 0.3 m/yr). In

2023, the deflation basins reached widths of 200-250 m (measured at 4 m MSL). The beach elevation, measured at 0-m distance, increased 0.9-1.2 m (1997-2023). Since 2021, the growth of embryo dunes on the beach, seaward of the new foredune, is evident at profile C1-C'1 and C2-C'2. Vegetation along the profiles emerged since 2017 or 2018 (*Figure 23*). It seems that vegetation primarily established in the deflation basins between the new foredunes and transgressive sand sheets, at elevations below 3 m MSL. However, in profile C1-C'1 vegetation also established above 7 m MSL (150-190 m). Once vegetation established, the vegetated area spatially increased and vegetation reached elevations above 3 m MSL (e.g. cross-section C1-C'1, 210-250 m). Vegetation established where dynamism is low; nearly all vegetation established where the depositional rate is below 0.3 m/yr and erosion is not occuring or less than 0.1 m/yr. Once vegetation established, the deposition in the succeeding years dropped to values below 0.1 m/yr.

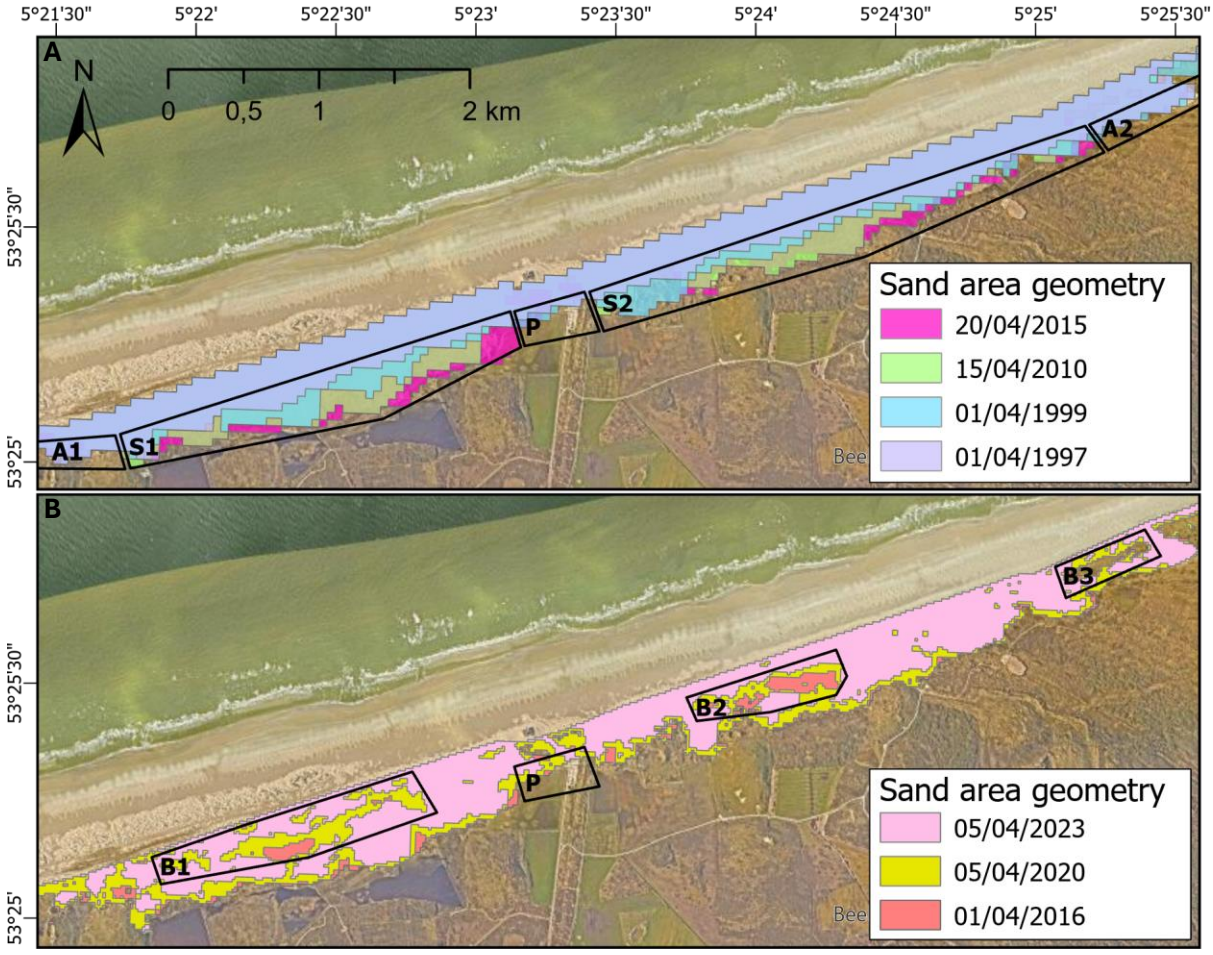

Figure 21. Sand surface area geometries (f_c>50%) within the BROI, equal to the rolling foredune and hinterland sections, (A) during the period when the sand surface area was increasing or stable (1997-2015) and (B) during the period when the sand surface area was decreasing (2016-2023). Black polygons indicate areas with limited sand drift (A1-2), landward sand drift (S1-2) and areas where vegetation (f_c>50%) established (B1-3). Polygon P indicates the area surrounding the parking lot.

Profiles C3-C'3 and C5-C'5 go through areas where vegetation has not re-established. Both profiles show the development of transgressive sand sheets seaward from the rolling foredune since 1997 and the formation of new foredunes seaward of the rolling foredune since 2004. Since

2007, deflation basin formed between the new foredunes and the landward migrating sand sheets. Over time the deflation basin decreased in elevation, reaching elevations around 3.5-4 m MSL. The deflation basin along the profiles is narrow and very dynamic. Erosional and depositional rates reach over 0.5 m/yr. The growth of embryo dunes did not occur along the profiles. The beach elevation, measures at 0-m distance, increased 0.8-0.9 m (1997-2023). Compared to the profiles along which vegetation re-established, the deflation basins have smaller cross-shore dimensions, are located at higher elevations, and exhibit greater dynamism.

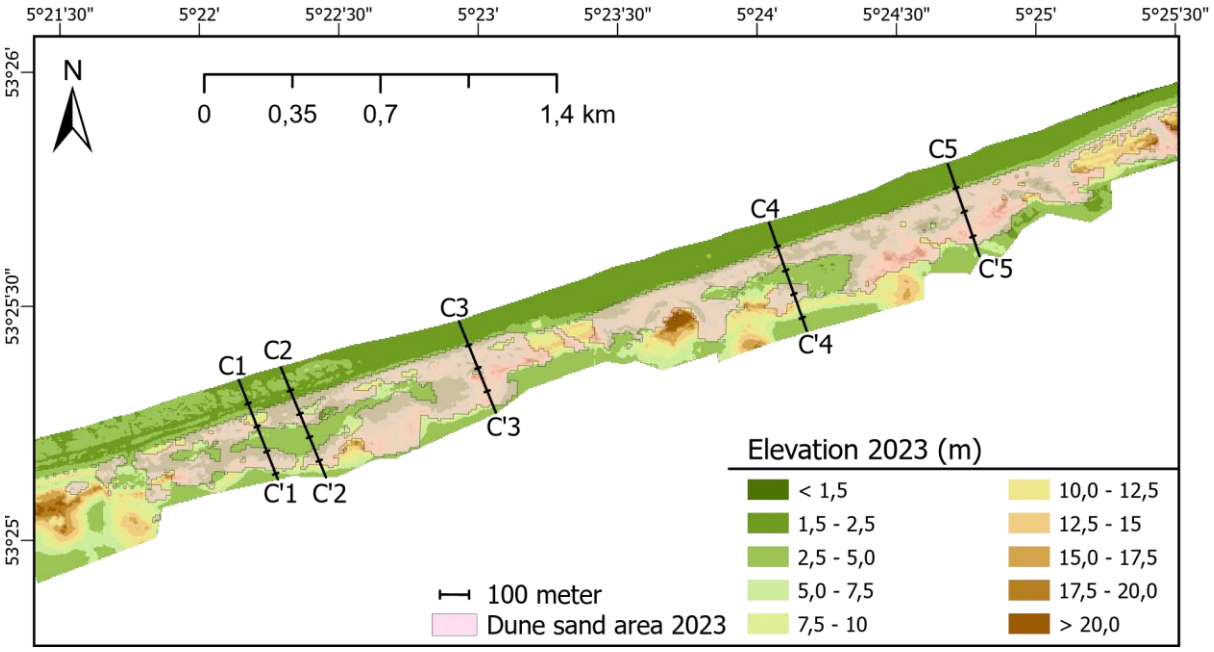

Figure 222. The locations of the cross-section profiles C1-C'1, C2-C'2, C3-C'3, C4-C'4 and C5-C'5, displayed on the 2023 sand surface area geometry and elevation map. Profiles C1-C'1, C2-C'2 and C4-C'4 go through areas where vegetation (f_c>50%) has re-established. Profiles C3-C'3 and C5-C'5 go through areas where vegetation has not re-established.

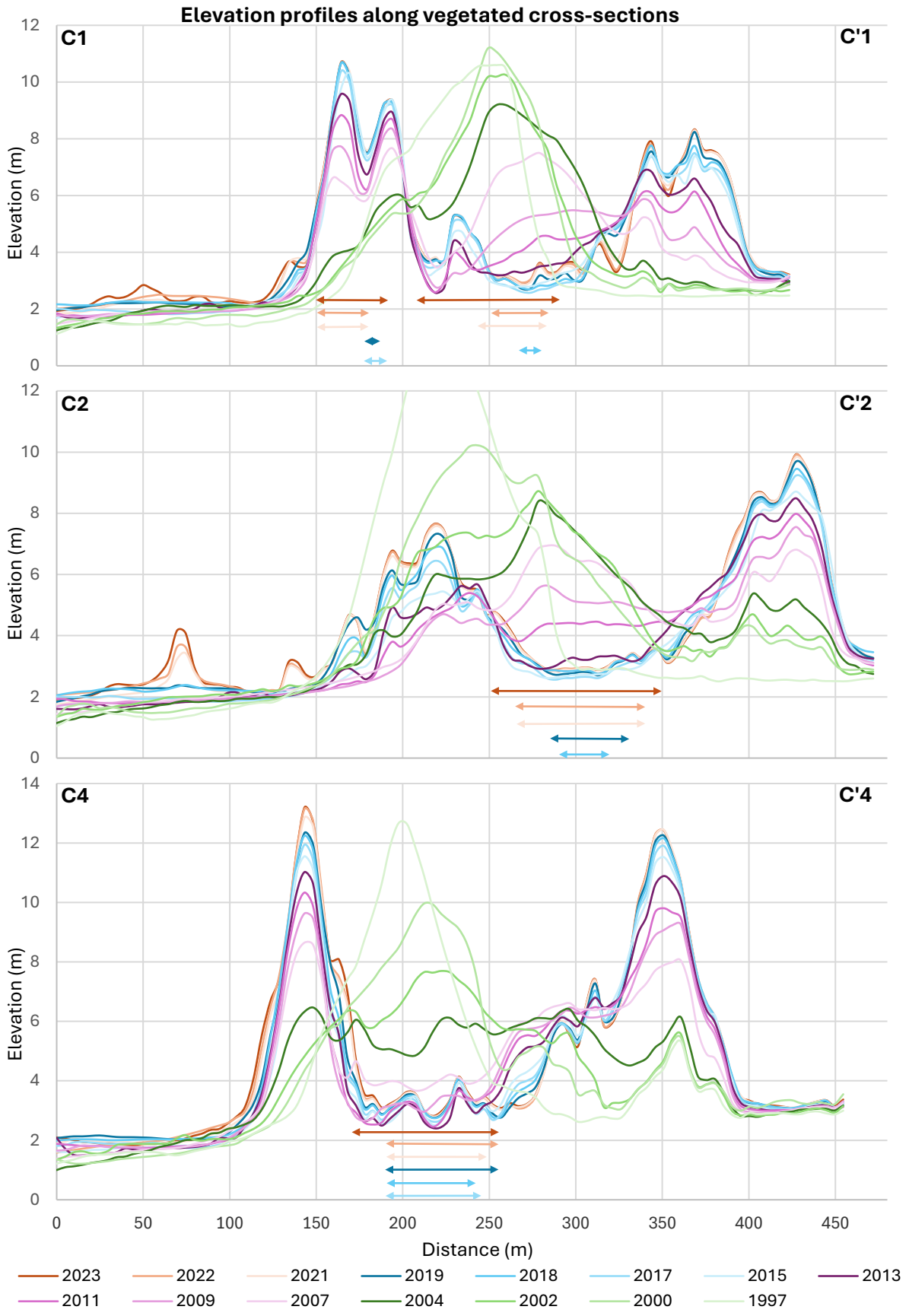

Figure 23. Elevation profiles along cross sections C1-C'1, C2-C'2 and C4-C'4. Vegetated areas (f_c>50%) along the profiles are indicated using arrows that match the colour scheme of the elevation profiles.

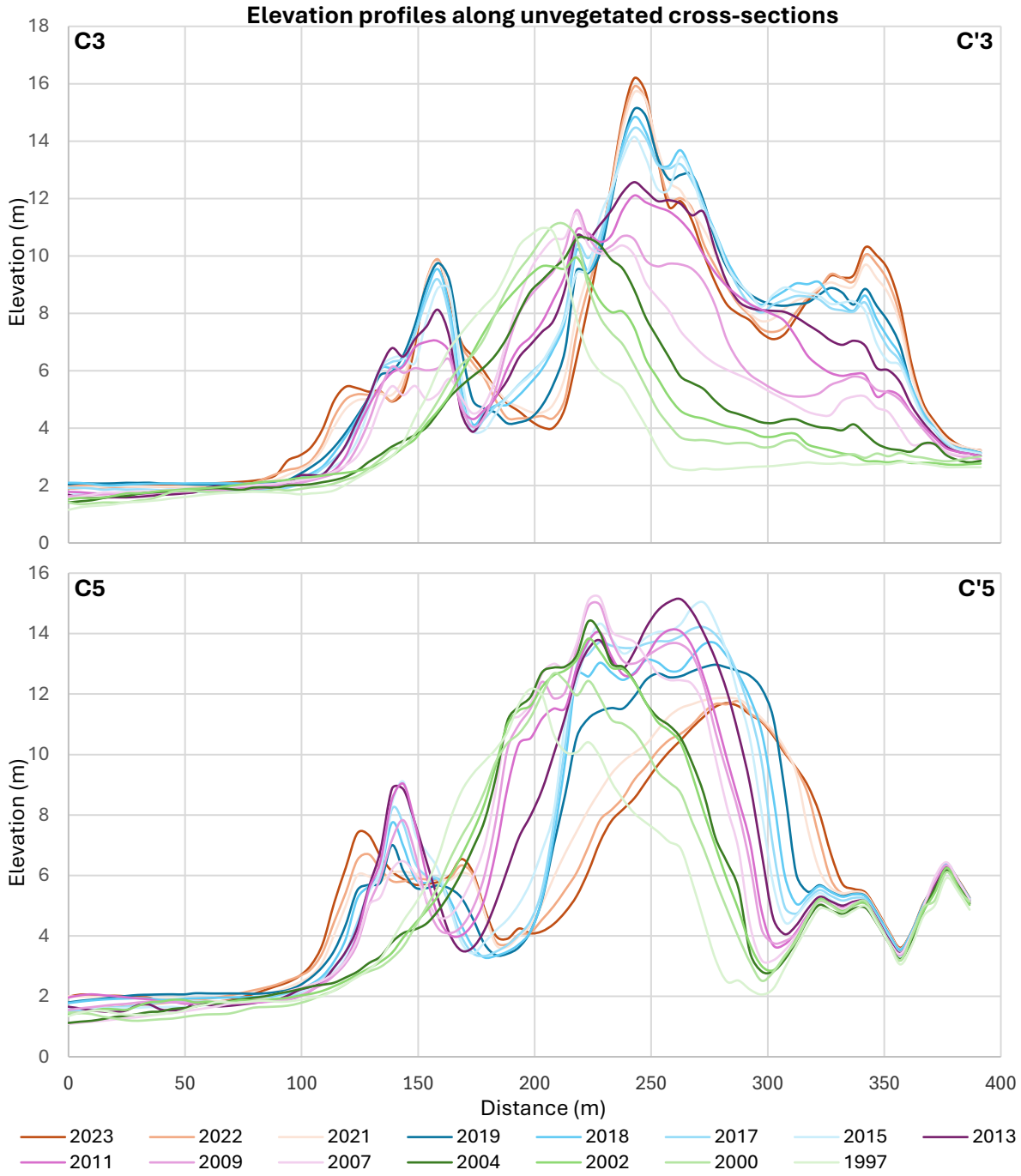

Figure 24. Elevation profiles along cross-sections C3-C'3 and C5-C'5.

6. Discussion

6.1. Physical processes

Although volumetric data prior to the implementation of the restoration measures is not available, observed trends in sand volume (*Figure 12*), absolute sand volume (*Figure 13*) and sand surface area (*Figure 20*) indicate that the restoration measures have increased dynamism. Because the restoration measures at Terschelling did not only involve the excavation of foredune notches through the unvegetated rolling foredune, but also the removal of sand trapping fences from it, dynamism increased along most of the foredune stretch (*Figure 14 and 21*). The only areas where sand drift was limited were the area surrounding the parking lot, where sand drift was likely artificially prevented, and the eastern and western sides of the rolling foredune, where sand drift was limited due to the high and vegetated hinterland (Appendix 2 and *Figure 21*). Aeolian processes eroded the rolling foredune and transported sand in both seaward and landward directions (*Figure 14, 23 and 24*). Sand from the rolling foredune, together with alongshore sediment input gradually formed new foredunes seaward of the rolling foredune and transgressive sand sheets landward of it. These initial developments resemble the geomorphological phase of the blowout development by Schwarz et al. (2019) (*Figure 3*). However, the development differs from dunefields where notches are excavated through vegetated foredunes. In the Zuid-Kennemerland dunefield (The Netherlands), for example, erosion occurred only in the deflation basin of the excavated notches as vegetation prevented erosion on the remainder of the foredune (e.g., Ruessink et al., 2018; van Kuik et al., 2022).

Rijkswaterstaat (2014) reported that the sand volume between RSP 15.5-18 (2500 m) increased ~11.625 m^3/m/yr (4.65×10^5 m^3) between 1997 and 2013. In the same time period, the sand volume between RSP 15-20 (4976 m), calculated in this study, increased ~10.7 m^3/m/yr (*Figure 12A*). The lower rate calculated by Rijkswaterstaat is likely the result of to the lower dynamics at the western (RSP 15-15.5) and eastern (RSP 18-20) edges of the dunefield (*Figure 14 and 21*), which were excluded from the volumetric calculations by Rijkswaterstaat (2014). Altogether, the volumetric data obtained in this study is expected to be in line with those of Rijkswaterstaat (2014).

The total sand supply between 2017 and 2018 (~63.6 m^3/m/yr) was over 5 times higher than to the average sand supply over the whole study period (~12.2 m^3/m/yr). Because the wind directions of the three strongest wind events between the 2017 and 2018 lidar surveys (Table 2) were favourable for alongshore sand transport into the study area, the relatively high sand supply is likely the result of these strong wind events. Additionally, given that the shore normal direction of the study area is 342° (*Figure 6*), winds during the 18 January 2018 wind event, the 8th largest storm in the Netherlands since 1970 (KNMI - Zware Stormen in Nederland Sinds 1910), were favourable for sand transport into the back dunes. However, while the storms resulted in an enormous alongshore sand input into the study area, the stabilization of the dunefield proceeded. The storms were thus not strong enough to cause an evolutionary stage reversal (*Figure 3*).

Table 2. The wind direction and maximum wind and wind surge speeds of three strongest wind events between the 2017 and 2018 lidar survey, measured by The Royal Netherlands Meteorological Institute, KNMI (KNMI - Zware Stormen in Nederland Sinds 1910, n.d.; KNMI - Zeer Zware Windstoten 13 September 2017, n.d.; KNMI - Code Rood Voor Zeer Zware Windstoten Op 18 Januari 2018, n.d.; KNMI - Code Oranje Voor Zeer Zware Windstoten Op 3 Januari 2018, n.d.).

Date	Max. wind speed (m/s)	Max. wind surge speed (m/s)	Wind direction
13/09/2017	26	35	S - SW
03/01/2018	26	34	S - W
18/01/2018	30	40	W - NW

Volumetric computations at the Zuid-Kennemerland dunefield by Ruessink et al. (2018) show that the alongshore sand supply into the study area was approximately 26.5 m^3/m/yr, from which 75% accumulated behind the foredune. Given that the dominant wind direction at the Zuid-Kennemerland dunes is similar to Terschelling (SW-W), the orientation of the Zuid-Kennemerland foredune, stretching NNE-SSW, is more optimal for sand transport through foredune notches compared to Terschelling. Because the rolling foredune sand at Terschelling transported in both seaward and landward directions, it is impossible to determine what percentage of the alongshore sand supply has been accumulating behind the foredune. Nonetheless, from 1997 to 2023, the sand volume in hinterland and rolling foredune sections combined gained ~6.2×10^5 m^3 (*Figure 12A*), which is 39% of the total volume increase within the study area (~15.8×10^5 m^3). This indicates that the restoration measures have been effectively increasing the sand volume in the back dunes.

6.2. Physical-ecological feedbacks

According to the conceptual model for blowout development by Swarz et al. (2019) (*Figure 3*), the physical activity within a blowout reduces once morphological funnelling through the blowout's deflation basin is reduced through erosion within the deflation basin. The decrease in physical activity will then allow for vegetation to establish and the foredune to regrow, causing the blowout to transition towards the bio-geomorphological stage. This resembles the development of the foredune at Terschelling. However, erosion at Terschelling did not only occur within the deflation basins of the excavated notches, but along most of the foredune stretch. Given that the alongshore sand input has been relatively constant (*Figure 12A*), the new foredune and beach growth limited the sand available for transport towards the hinterland. Therefore, aeolian erosion created deflation basins between the new foredunes and transgressive sand sheets. These basins reached depths of approximately 2.5 - 3 m MSL (*Figure 23*). Similar erosion in deflation basins described by Hesp and Walker (2013) and Hesp (2024), erosion in the basins ceased at 2.5 - 3 m MSL because the ground was saturated due to its proximity to the water table.

Since 2017, vegetation (f_c>50%) has established within the deflation basins and has been spatially increasing in size. Vegetation reached such high covers because conditions within the deflation basins became favourable for vegetation to thrive. Cross-sections combined with sand surface area geometries reveal that vegetation mainly established below 3 m MSL, where depositional and erosional rates are below 0.3 and 0.1 m/yr, respectively (*Figure 23*). The lower elevations facilitated easier (ground)water excess and exhibited higher moisture levels (e.g., Gao

et al., 2023). Additionally, the formation of strong root and rhizome systems provided greater resistance to suboptimal conditions compared to newly establishing vegetation (Keijsers et al., 2015). The growth of rhizome systems and higher moisture levels in the vegetated patches allowed vegetation to expand upslope gradually (e.g., Liu et al., 2012; Gao et al., 2023). Vegetation has also established on higher elevations (*Figure 23, profile C1-C'1*), thus further away from water table. Here, the erosional and depositional rates are also below 0.1 and 0.3 m/yr, respectively. For vegetation establishment, low dynamism is therefore arguably more important than low elevation and proximity to the water table. The observed erosional and depositional rates fall within the observed range of sedimentation within vegetation on Ameland, the barrier island eastward of Terschelling, by Keijsers et al. (2015), being −0.2 to 0.7 m/year at 50% vegetation cover. The observed maximum depositional rate is also similar to the ideal deposition rate for marram grass, ~0.3 m/yr, and below the maximum burial rate, ~0.85 m/yr, found by Nolet et al. (2018).

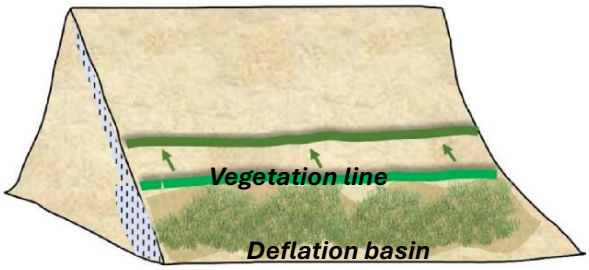

Figure 25. Illustration of vegetation growth in a deflation basin and vegetation expanding upslope. From: Gao et al. (2023).

Not all blowouts become vegetated and inactive. At Skodbjerge (Denmark), for example, where blowouts have been active for over 40 years (van Kuik et al., 2022), continued coastal erosion and retreat (1 m/yr) have been preventing prevent coastal stabilization and foredune formation (Sørensen and Karlsson, 2022). Similarly, at l'Anse du Gurp (France), where blowouts have been active for over 80 years, coastal erosion and retreat (1.26 m/yr) have also been preventing stabilization and foredune growth (Laporte-Fauret et al., 2022). Both Skodbjerge and l'Anse du Gurp are natural eroding and dynamic systems where blowouts naturally occur (*Figure 1, box B and C*). At Terschelling, however, the positive sediment input created a high and wide beach (*Figure 23 and 24,* Appendix 4), where foredune scarping during storms does not occur. Therefore, Terschelling is a stabilizing system with a prograding coastline, where blowouts do not naturally occur (*Figure 1, box A*). If the sediment budged at Terschelling had been negative and the coastline had retreated, the dunefield would have developed more similar to Skodbjerge or l'Anse du Gurp.

Overall, the results reveal that the dunefield at Terschelling is characterized by growth, stabilization, and decay, resembling the geomorphological, bio-geomorphological, and ecological stages in Schwarz et al. (2019)'s conceptual model of blowout development (*Figure 3*). The dunefield gradually progressed from the geomorphological to the ecological stage due to beach progradation and new foredune growth. Because the system gradually transitioned through the stages, exact timings of the stage transitions can not be pinpointed. Continued vegetation growth is expected to stabilize the entire system over time. Because the dunefield is not characterized by coastal erosion and other dynamics that typically stimulate dune activity, the foredune and hinterland will likely revegetate and restabilize completely.

6.3. Limitations and future development

The GEE algorithm developed by van Kuik et al., (2022) produced a sand surface area time series with many outliers and a reversed seasonal pattern. This output was unexpected, as time series produced by van Kuik et al. (2022) did not exhibit these issues. The inverted seasonality can possible be resolved by applying a fixed Otsu threshold. Testing this approach, however, was not feasible within timeframe of this thesis. When the algorithm functions correctly and time series with a correct seasonal pattern are produced, it can be useful for assessing the spatial development of the sand surface area within a dunefield with high temporal resolution (van Kuik et al., 2022). Because this study was limited to only one sand surface area geometry and elevation map per year, the effect of seasonal changes and episodic events could not be evaluated. Only the combined impact of three large episodic wind events, occuring between two adjacent lidar surveys, could be recognized in the sand volume development. Furthermore, because the algorithm is designed to detect sand with a fractional cover above 50%, it overlooks initial vegetation establishment. By testing lower fractional covers, earlier vegetation establishment can be studied. However, to properly assess vegetation establishment imagery with a finer resolution is recommended.

Observations reveal that vegetation is re-establishing not only within the deflation basins, but in most parts of the restored dunefield. Further greening and stabilization of the dunefield is expected due to a variety of reasons. Firstly, the dynamics in the dunefield have been decreasing. This includes the decrease in erosion and deposition, being able to destroy of suffocate vegetation. Secondly, higher groundwater and moisture levels in the dunefield (Rijkswaterstaat, 2014) favour vegetation growth and result in less aeolian transport (e.g., Bauer et al., 2009). Thirdly, climate change causes the growing season to be prolonged (Arens et al., 2013; Provoost et al., 2011), providing more time for vegetation to grow. There are no indications that mobility is or will increase naturally. To reintroduce dynamism, new restoration measures are therefore required.

7. Conclusions

The evolution of the restored dunefield at middle Terschelling was visualized and quantified using lidar data and freely available satellite imagery. Time series of sand volume, absolute sand volume and sand surface area indicate that the excavation of foredune notches and the removal of sand trapping fences in 1995 led to remarkable dynamism. Aeolian erosion and transportation of sand from the rolling foredune in both landward and seaward direction, together with a positive alongshore sand input from the beach, gradually created new foredunes and transgressive sand sheets. Over time, sand deposition on and seaward of the new foredunes reduced sand transport into the back dunes, and aeolian erosion formed deflation basins between the new foredunes and transgressive sand sheets. The deflation basins eroded until grounds that were saturated due to their proximity to the water table were reached. The proximity to the water table and limited erosion allowed vegetation to establish. Vegetation (f_c> 50%) emerged since 2017, mostly within the deflation basins, at elevations below 3 m MSL, where the depositional and erosional rates were below 0.3 and 0.1 m/yr, respectively. This indicates that vegetation expansion in the dunefield is mainly regulated by the geomorphological evolution, dynamism and topography of the dunefield. The total alongshore sand transport into the study area was ~15.8×10^5 m^3 (~12.2 m^3/m/yr). Although most sand has accumulated on and seaward of the new foredune, the sand volume in the back dunes increased ~6.2×10^5 m^3, being 39% of the total alongshore sand budget. While storms greatly increased the alongshore sand budged, they did not cause foredune erosion and reactivation of dynamics.

In 28 years, the restored dunefield at middle Terschelling has transitioned from a highly dynamic to a more stable and vegetated state. This does not imply that the project has failed. On the contrary, the stabilization and greening represent natural evolutionary processes driven by intrinsic feedback mechanisms between geomorphological processes and vegetation dynamics. In a region without coastal erosion or other processes that typically stimulate dune dynamics, restored dunefields are likely to restabilize. Once an ecosystem restabilizes, new restoration measures are required to reintroduce dynamics, especially if natural foredune scarping during storms does not occur because of a high and wide beach. Overall, this study highlights the intricate and evolving nature of coastal dune ecosystems, emphasizing the importance of long-term monitoring to understand and predict changes in restored dynamic coastal environments. Future monitoring and research are required to study seasonal volumetric and areal changes and to assess how initial vegetation establishment is related to the geomorphological evolution, dynamism and topography of a restored dunefield.

References

Angus, S. (2001). The Outer Hebrides, volume 2: Moor and Machair. White Horse, Cambridge

Arens, S. M., Slings, Q., & De Vries, C. N. (2004). Mobility of a remobilised parabolic dune in Kennemerland, The Netherlands. Geomorphology, 59(1-4), 175-188.

Arens, S. M., Van Kaam-Peters, H. M. E., & Van Boxel, J. H. (1995). Air flow over foredunes and implications for sand transport. Earth surface processes and landforms, 20(4), 315-332.

Arens, S. M., Löffler, M.A.M., & Nuijen, E.M. (2007). Evaluatie dynamisch kustbeheer Friese Waddeneilanden. Arens Bureau voor Strand- en Duinonderzoek, RAP2006.04, 74 pp

Arens, S. M., Mulder, J. P., Slings, Q. L., Geelen, L. H., & Damsma, P. (2013). Dynamic dune management, integrating objectives of nature development and coastal safety: Examples from the Netherlands. Geomorphology, 199, 205-213.

Arens, S. M., Slings, Q. L., Geelen, L. H., & Van der Hagen, H. G. (2013). Restoration of dune mobility in the Netherlands. In Restoration of coastal dunes (pp. 107-124). Berlin, Heidelberg: Springer Berlin Heidelberg.

Bakker, T. W., & Stuyfzand, P. J. (1993). Nature conservation and extraction of drinking water in coastal dunes: the Meijendel area. In Landscape Ecology of a Stressed Environment (pp. 244-262). Dordrecht: Springer Netherlands.

Bauer, B. O., Davidson-Arnott, R. G. D., Hesp, P. A., Namikas, S. L., Ollerhead, J., & Walker, I. J. (2009). Aeolian sediment transport on a beach: Surface moisture, wind fetch, and mean transport. Geomorphology, 105(1-2), 106-116.

Blanco, P. D., Rostagno, C. M., Del Valle, H. F., Beeskow, A. M., & Wiegand, T. (2008). Grazing impacts in vegetated dune fields: predictions from spatial pattern analysis. Rangeland ecology & management, 61(2), 194-203.

Bochev-Van der Burgh, L. M., Wijnberg, K. M., & Hulscher, S. J. (2011). Decadal-scale morphologic variability of managed coastal dunes. Coastal engineering, 58(9), 927-936.

Daniel Pereira (2024). Wind Rose (https://www.mathworks.com/matlabcentral/fileexchange/47248-wind-rose), MATLAB Central File Exchange. Retrieved May 18, 2024.

De Ruig, J. H., & Hillen, R. (1997). Developments in Dutch coastline management: Conclusions from the second governmental coastal report. Journal of Coastal Conservation, 3, 203-210.

De Schipper, M. A., Ludka, B. C., Raubenheimer, B., Luijendijk, A. P., & Schlacher, T. A. (2021). Beach nourishment has complex implications for the future of sandy shores. Nature Reviews Earth & Environment, 2(1), 70-84.

De Groen, F., V. van Zelst, L. van der Valk & B. Arens (2019). Natuurlijk Veilig door Kust- en Zeereep-beheer Deltares rapport 11203683-002-ZKS-0014.

Elko, N., Briggs, T. R., Benedet, L., Robertson, Q., Thomson, G., Webb, B. M., & Garvey, K. (2021). A century of US beach nourishment. Ocean & Coastal Management, 199, 105406.

Environmental Systems Research Institute (ESRI). (2024). ArcGIS Release 3.1.2. Redlands, CA.

Gares, P. A. (1992). Topographic changes associated with coastal dune blowouts at Island Beach State Park, New Jersey. Earth Surface Processes and Landforms, 17(6), 589-604.

Gares, P. A., & Nordstrom, K. F. (1995). A Cyclic Model of Foredune Blowout Evolution for a Leeward Coast : Island Beach, New Jersey. Annals of the Association of Amercan Geographers, 85(1), 1–20.

Gao, J., Kennedy, D. M., & Konlechner, T. M. (2020). Coastal dune mobility over the past century: A global review. Progress in Physical Geography: Earth and Environment, 44(6), 814-836.

Gao, J., Kennedy, D. M., & McSweeney, S. (2023). Patterns of vegetation expansion during dune stabilization at the decadal scale. Earth Surface Processes and Landforms, 48(15), 3059-3073.

Goff, J. R., Lane, E., & Arnold, J. (2009). The tsunami geomorphology of coastal dunes. Natural Hazards and Earth System Sciences, 9(3), 847-854.

Graffin, M., Regard, V., Carretier, S., Maffre, P., & Almar, R. (2021). On the overlooked impact of river dams on beach erosion worldwide.

Hanley, M. E., Hoggart, S. P. G., Simmonds, D. J., Bichot, A., Colangelo, M. A., Bozzeda, F., ... & Thompson, R. C. (2014). Shifting sands? Coastal protection by sand banks, beaches and dunes. Coastal Engineering, 87, 136-146.

Hanson, H., Brampton, A., Capobianco, M., Dette, H. H., Hamm, L., Laustrup, C., ... & Spanhoff, R. (2002). Beach nourishment projects, practices, and objectives—a European overview. Coastal engineering, 47(2), 81-111.

Hesp, P. A. (2013). Conceptual models of the evolution of transgressive dune field systems. Geomorphology, 199, 138-149.

Hesp, P. A., Davidson-Arnott, R., Walker, I. J., & Ollerhead, J. (2005). Flow dynamics over a foredune at Prince Edward Island, Canada. Geomorphology, 65(1-2), 71-84.

Hesp, P. (2002). Foredunes and blowouts: initiation, geomorphology and dynamics. Geomorphology, 48(1-3), 245-268.

Hesp, P. A., & Hilton, M. J. (2013). Restoration of foredunes and transgressive dunefields: case studies from New Zealand. In Restoration of coastal dunes (pp. 67-92). Berlin, Heidelberg: Springer Berlin Heidelberg.

Hesp, P. A., & Hyde, R. (1996). Flow dynamics and geomorphology of a trough blowout. Sedimentology, 43(3), 505-525.

Hesp, P. A., & Walker, I. J. (2013). Coastal dunes. In Aeolian Geomorphology (pp. 328-355). Elsevier Inc.

Hesp, P. A. (1989). A review of biological and geomorphological processes involved in the initiation and development of incipient foredunes. Proceedings of the Royal Society of Edinburgh, Section B: Biological Sciences, 96, 181-201.

Hesp, Patrick & Smyth, Thomas & Walker, Ian & Gares, Paul & Wasklewicz, Thad. (2016). Flow within a Trough Blowout at Cape Cod. Journal of Coastal Research. 75. 288-292. 10.2112/SI75-058.1.

Jackson, D. W., Costas, S., González-Villanueva, R., & Cooper, A. (2019). A global 'greening'of coastal dunes: An integrated consequence of climate change?. Global and Planetary Change, 182, 103026.

Jewell, M., Houser, C., & Trimble, S. (2017). Phases of blowout initiation and stabilization on Padre Island revealed through ground-penetrating radar and remotely sensed imagery. Physical Geography, 38(6), 556-577.

Keijsers, J. G., Giardino, A., Poortinga, A., Mulder, J. P., Riksen, M. J., & Santinelli, G. (2015). Adaptation strategies to maintain dunes as flexible coastal flood defense in The Netherlands. Mitigation and adaptation strategies for global change, 20, 913-928.

Keijsers, J. G. S., De Groot, A. V., & Riksen, M. J. P. M. (2015). Vegetation and sedimentation on coastal foredunes. Geomorphology, 228, 723-734.

NMI - Code oranje voor zeer zware windstoten op 3 januari 2018. (n.d.). https://www.knmi.nl/kennis-en-datacentrum/achtergrond/Code-oranje-voor-zeer-zware-windstoten-op-3-januari-2018.

KNMI - Code rood voor zeer zware windstoten op 18 januari 2018. (n.d.). https://www.knmi.nl/kennis-en-datacentrum/achtergrond/code-rood-voor-zeer-zware-windstoten-op-18-januari.

KNMI - Zeer zware windstoten 13 september 2017. (n.d.). https://www.knmi.nl/kennis-en-datacentrum/achtergrond/zeer-zware-windstoten-13-september-2017.

KNMI - Zware stormen in Nederland sinds 1910. (n.d.). https://www.knmi.nl/nederland-nu/klimatologie/lijsten/zwarestormen

Laporte-Fauret, Q., Castelle, B., Marieu, V., Nicolae-Lerma, A., & Rosebery, D. (2022). Foredune blowout formation and subsequent evolution along a chronically eroding high-energy coast. Geomorphology, 414, 108398.

Laporte-Fauret, Q., Castelle, B., Michalet, R., Marieu, V., Bujan, S., & Rosebery, D. (2021). Morphological and ecological responses of a managed coastal sand dune to experimental notches. Science of the Total Environment, 782, 146813.

LAStools, "Efficient LiDAR Processing Software" (version 240213, unlicenced), obtained from http://rapidlasso.com/LAStools

Levin, N., Jablon, P. E., Phinn, S., & Collins, K. (2017). Coastal dune activity and foredune formation on Moreton Island, Australia, 1944–2015. Aeolian research, 25, 107-121.

Liu, B., Liu, Z., & Wang, L. (2012). The colonization of active sand dunes by rhizomatous plants through vegetative propagation and its role in vegetation restoration. Ecological Engineering, 44, 344-347.

Löffler, M.A.M.; Leeuw, C.C. de; Haaf, M.E. Ten; Verbeek, S.K.; Oost, A.P.; Grootjans, A.P.; Lammerts, E.J. & Haring, R.M.K. (2008) Eilanden natuurlijk. Natuurlijke dynamiek en veerkracht op de Waddeneilanden. Het tij geleerd (samenwerkingsverband), ISBN 9789070322304.

Lopez, A. C. B., & Hesp, P. A. (2023). Evolution of a coastal transgressive dunefield to a parabolic dunefield, Canunda dunes, South Australia. Geomorphology, 430, 108653.

Martínez, L. M., Gallego-Fernández, J. B., & Hesp, P. A. (Eds.). (2013). Restoration of coastal dunes.

Martínez, M. L., & Psuty, N. P. (2004). Coastal dunes. Berlin: Springer Verlag.

Maun, M. A. (1998). Adaptations of plants to burial in coastal sand dunes. Canadian Journal of Botany, 76(5), 713-738.

Meijer, J., Vriens, G. & Lammerts, E. J., 2016. Natura 2000-beheerplan Terschelling (4).

Ministerie van Verkeer en Waterstaat, 1996. Kustbalans 1995 - de tweede kustnota. Directoraat Generaal Rijkswaterstaat april 1996.

Nguyen, D., Hilton, M., & Wakes, S. (2022). Aeolian sand transport thresholds in excavated foredune notches. Earth Surface Processes and Landforms, 47(2), 553-568.

Nguyen, D. M. (2022). Wind flow dynamics and sand transport through excavated foredune notches (Doctoral dissertation, University of Otago).

Noordstra, P. (1991). Analyse zeereep Terschelling (RSP 15 - 20). Rapport ANW 91.41

Nordstrom, K. F., & Arens, S. M. (1998). The role of human actions in evolution and management of foredunes in The Netherlands and New Jersey, USA. Journal of Coastal Conservation, 4, 169-180.

Nordstrom, K. F., & Jackson, N. L. (2013). Foredune restoration in urban settings. In Restoration of coastal dunes (pp. 17-31). Berlin, Heidelberg: Springer Berlin Heidelberg.

Nordstrom, K. F., & Lotstein, E. L. (1989). Perspectives on resource use of dynamic coastal dunes. Geographical review, 1-12.

Nordstrom, K. F., Hartman, J., Freestone, A. L., Wong, M., & Jackson, N. L. (2007). Changes in topography and vegetation near gaps in a protective foredune. Ocean & Coastal Management, 50(11-12), 945-959.

Nolet, C., Van Puijenbroek, M., Suomalainen, J., Limpens, J., & Riksen, M. (2018). UAV-imaging to model growth response of marram grass to sand burial: Implications for coastal dune development. Aeolian Research, 31, 50-61.

Nolet, C., & Riksen, M. J. (2019). Accommodation space indicates dune development potential along an urbanized and frequently nourished coastline. Earth Surface Dynamics, 7(1), 129-145.

Olson, J.S., Van der Maarel, E., 1989. Coastal dunes in Europe: a global view. In. Van der Meulen, F., Jungerius, P.D., Visser, J.H. (Eds), Perspectives in Coastal Dune Management. The Hague: SPB Academic Publishing, pp. 3-32.

POK, 1998. Dynamisch kustbeheer: midden en oostelijk Terschelling. Een advies over het kustbeheer van paal 8 tot paal 26 op Terschelling. Provinciaal Overlegorgaan Kust Friesland, projectgroep Terschelling. Mei 1998.

Popescu, S. C. (2011). Lidar remote sensing. Advances in environmental remote sensing: Sensors, algorithms, and applications, 450, 59-60.

Pye, K., & Blott, S. J. (2016). Assessment of beach and dune erosion and accretion using LiDAR: Impact of the stormy 2013–14 winter and longer term trends on the Sefton Coast, UK. Geomorphology, 266, 146-167.

Pye K, Blott S (2017) Evolution of a sediment-starved, over-stabilised dunefield: Kenfig Burrows, South Wales, UK. Journal of Coastal Conservation 21: 685–717.

Quataert, E., A. Oost, M. Hijma & E. Elias. 2020 Beheerbibliotheek Terschelling. Deltaresrapport 11205236-001-ZKS-0002 https://edepot.wur.nl/548412.

Ranwell, D. S. (1960). Newborough Warren, Anglesey: III. Changes in the vegetation on parts of the dune system after the loss of rabbits by myxomatosis. The Journal of Ecology, 385-395.

Rijkswaterstaat, & Staatsbosbeheer. (2015). Een levend duinlandschap op Terschelling Duurzame bescherming voor mens en natuur.

Rijkswaterstaat, Staatsbosbeheer, & Vitens. (2014). Notitie Ontwikkelingen kustvak paal 15-20 op Terschelling.

Roeland, H., & Piet, R. (1995). Dynamic preservation of the coastline in the Netherlands. Journal of Coastal Conservation, 1, 17-28.

Sawakuchi, A. O., Kalchgruber, R., Giannini, P. C. F., Nascimento Jr, D. R., Guedes, C. C. F., & Umisedo, N. K. (2008). The development of blowouts and foredunes in the Ilha Comprida barrier (Southeastern Brazil): the influence of Late Holocene climate changes on coastal sedimentation. Quaternary Science Reviews, 27(21-22), 2076-2090.

Schwarz, C., Van Starrenburg, C., Donker, J., & Ruessink, G. (2021). Wind and sand transport across a vegetated foredune slope. Journal of Geophysical Research: Earth Surface, 126(1), e2020JF005732.

Stuivende duinen. (n.d.). VVV Terschelling. https://www.vvvterschelling.nl/bedrijven/stuivende-duinen/

Stuyfzand, P.J., Arens, S.M., Oost, A.P. (2010). Geochemische effecten van zandsupletie langs Hollands kust. Bosschap, bedrijfschap voor bos en natuur.

Sumption, K. J., & Flowerdew, J. R. (1985). The ecological effects of the decline in rabbits (Oryctolagus cuniculus L.) due to myxomatosis. Mammal Review, 15(4), 151-186.

Tasseled Cap Transformation for Landsat 8 and 9. (2023). From: https://supportsi.hexagon.com/help/s/article/Tasseled-Cap-Transformation-for-Landsat-8?language=en_US

The development of a digital terrain model for the geomorphological engineering of the ‘rolling’ foredune of Terschelling, the Netherlands van der Wal, D

Van Boxel, J. H., Jungerius, P. D., Kieffer, N., & Hampele, N. (1997). Ecological effects of reactivation of artificially stabilized blowouts in coastal dunes. Journal of Coastal Conservation, 3, 57-62.

Van der Meulen, F., & Salman, A. H. P. M. (1996). Management of Mediterranean coastal dunes. Ocean & Coastal Management, 30(2-3), 177-195.

Van Dijk, H. W. J. (1989). Ecological impact of drinking-water production in Dutch coastal dunes.

Van der Maarel, E., Boot, R., van Dorp, D., & Rijntjes, J. (1985). Vegetation succession on the dunes near Oostvoorne, The Netherlands; a comparison of the vegetation in 1959 and 1980. Vegetatio, 58, 137-187.

Van Kuik, N., de Vries, J., Schwarz, C., & Ruessink, G. (2022). Surface-area development of foredune trough blowouts and associated parabolic dunes quantified from time series of satellite imagery. Aeolian Research, 57, 100812.

Voorbeelden van Dynamisch Kustbeheer. Deltares, 2013, B dr. L. van der Valk J. Reinders MSc dr. A.J.F. van der Spek drs. C. van Gelder-Maas.dr. A.J.F. van der Spek drs. C. van Gelder-Maas.

Wind and weather statistic Terschelling Hoorn. (n.d.). Windfinder.com. https://nl.windfinder.com/windstatistics/terschelling

Appendices

Appendix 1. Additional rolling foredune imagery

Appendix 1. Rolling foredune imagery from 1987 (Rijkswaterstaat en Staatsbosbeheer, 2015).

Appendix 2. Elevation models

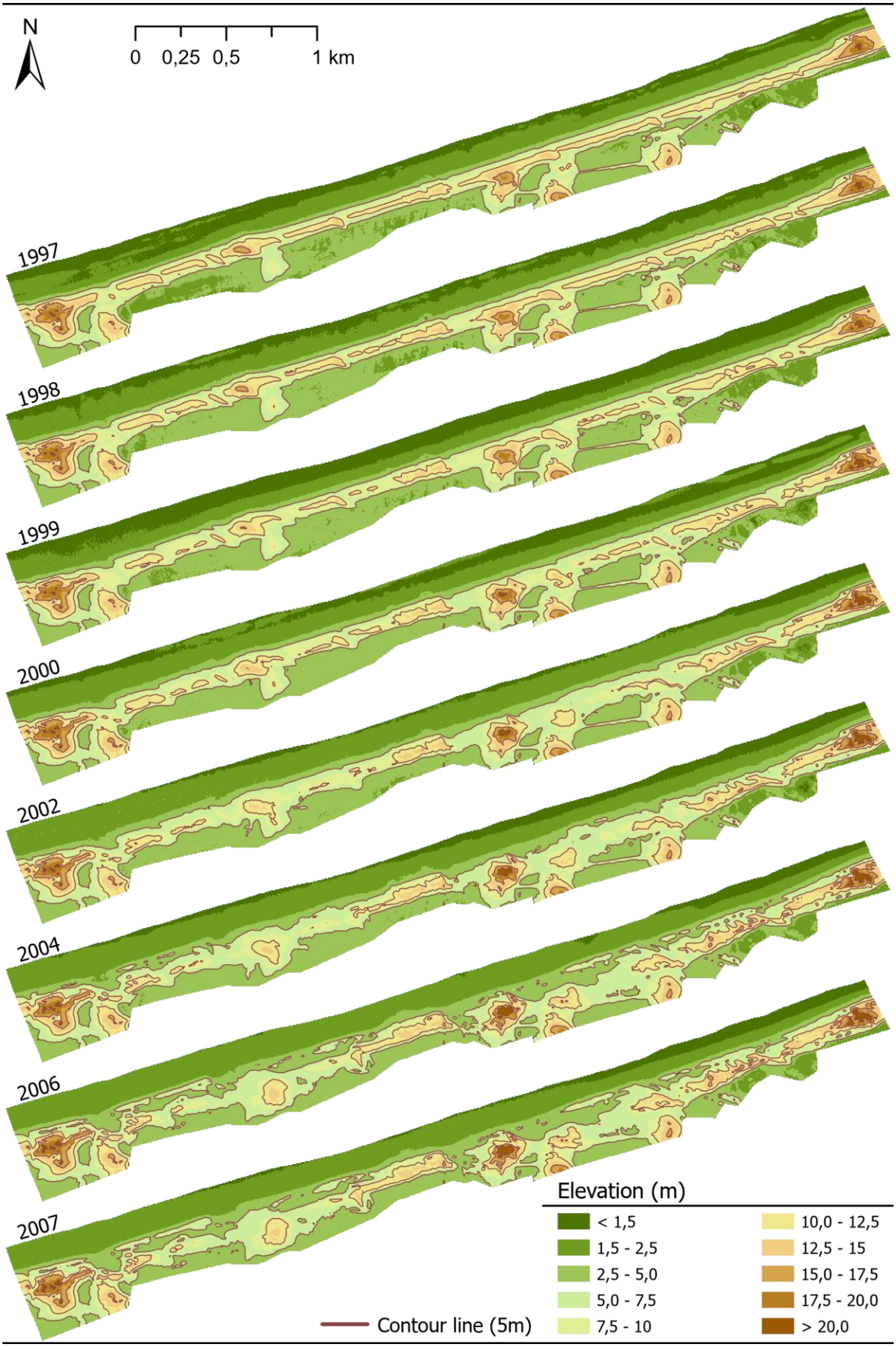

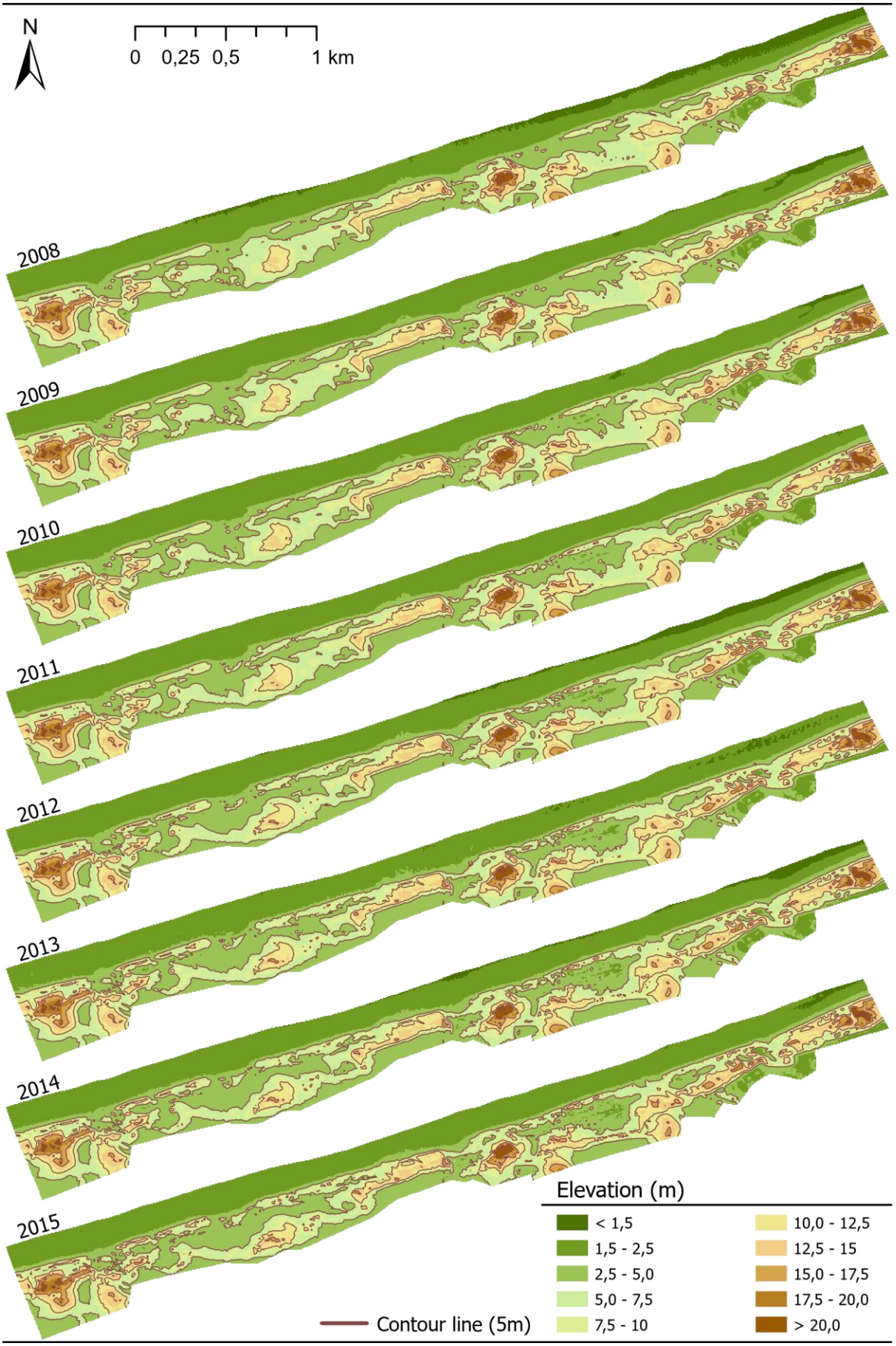
N
0 0,25 0,5 1 km
2008
2009
2010
2011
2012
2013
2014
2015
Elevation (m)
< 1,5
1,5 - 2,5
2,5 - 5,0
5,0 - 7,5
7,5 - 10
10,0 - 12,5
12,5 - 15
15,0 - 17,5
17,5 - 20,0
> 20,0
Contour line (5m)

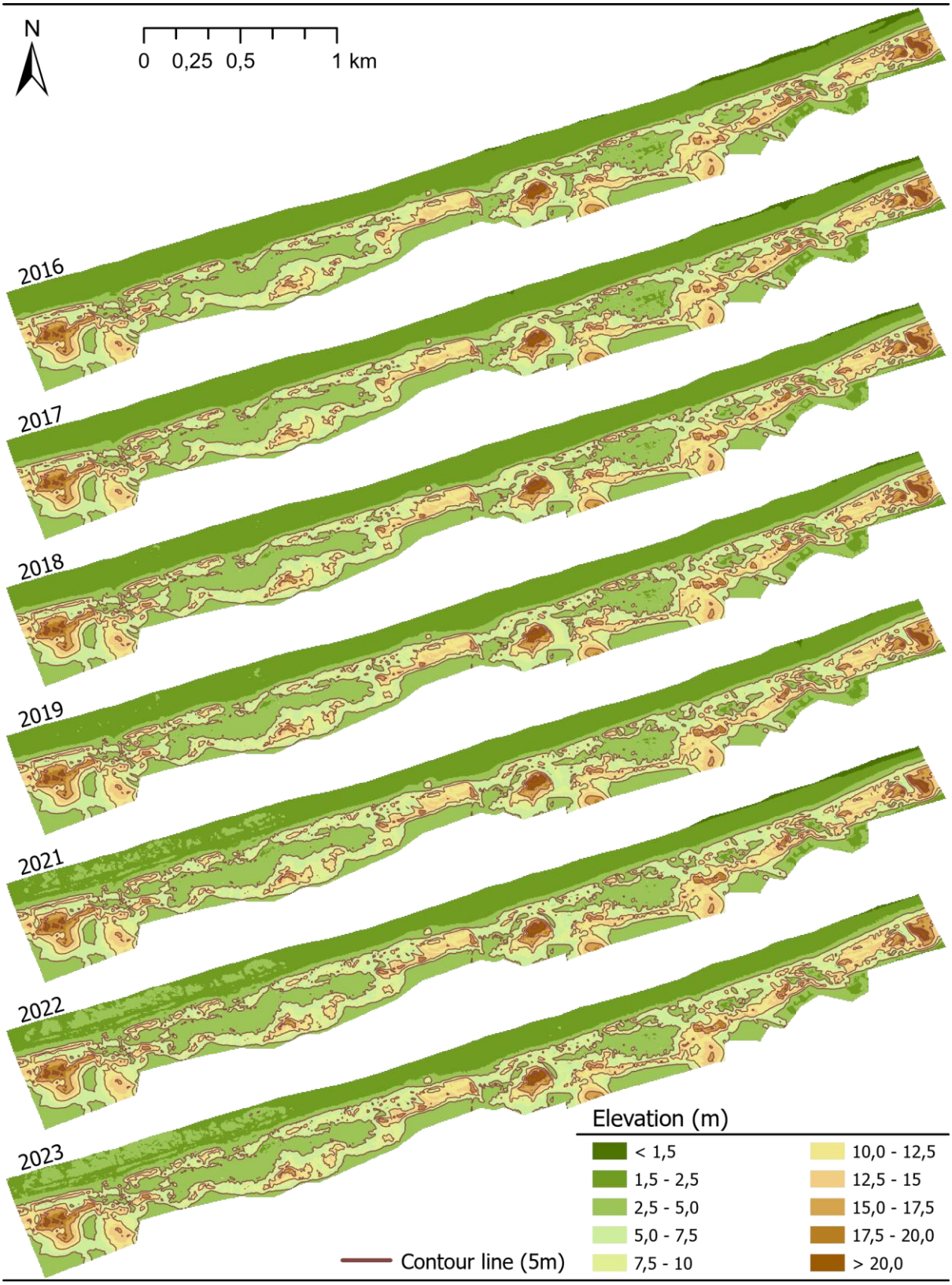

Appendix 2. Elevation models with 5-meter contour line interval.

Appendix 3. Elevation difference models

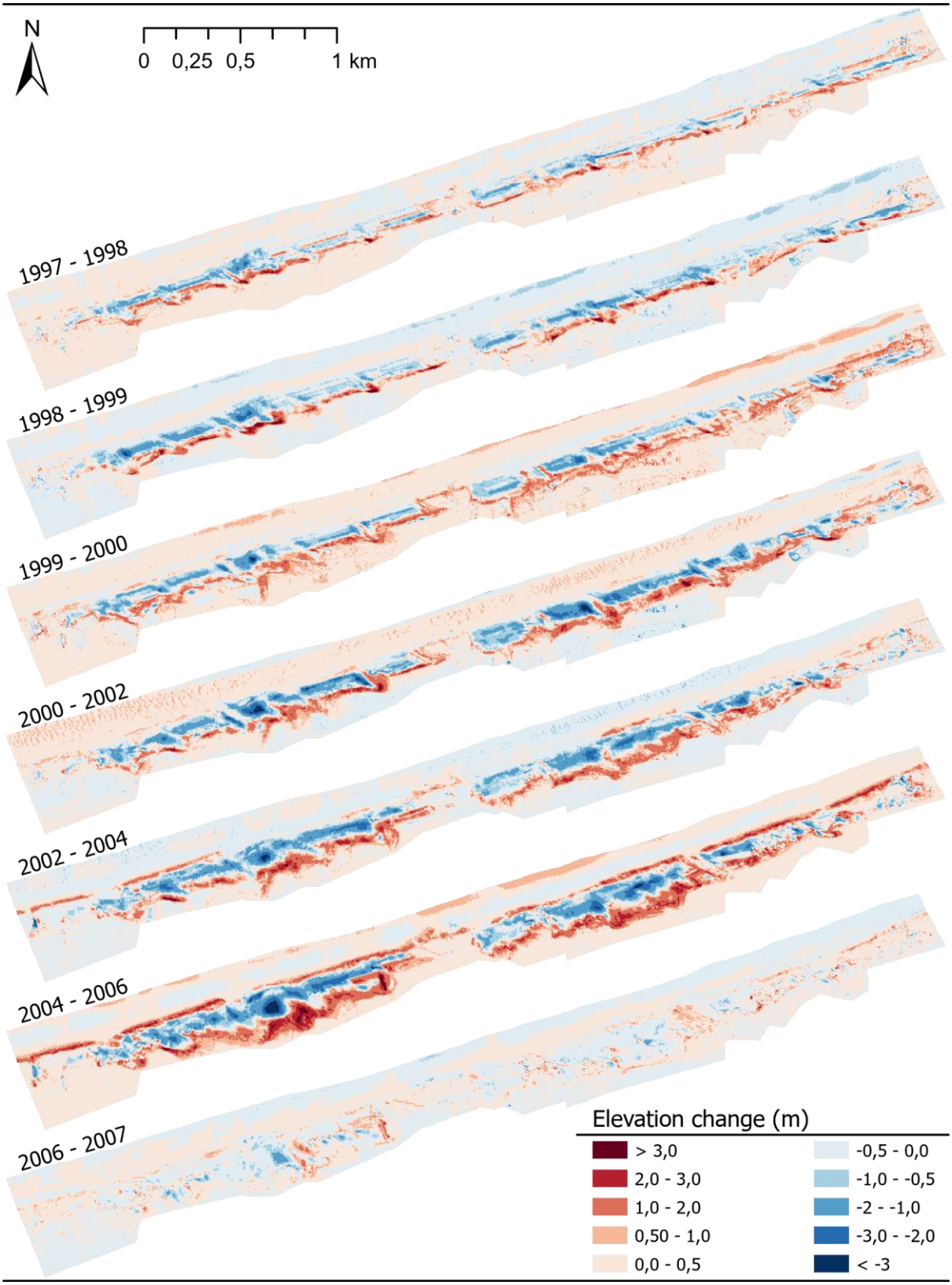

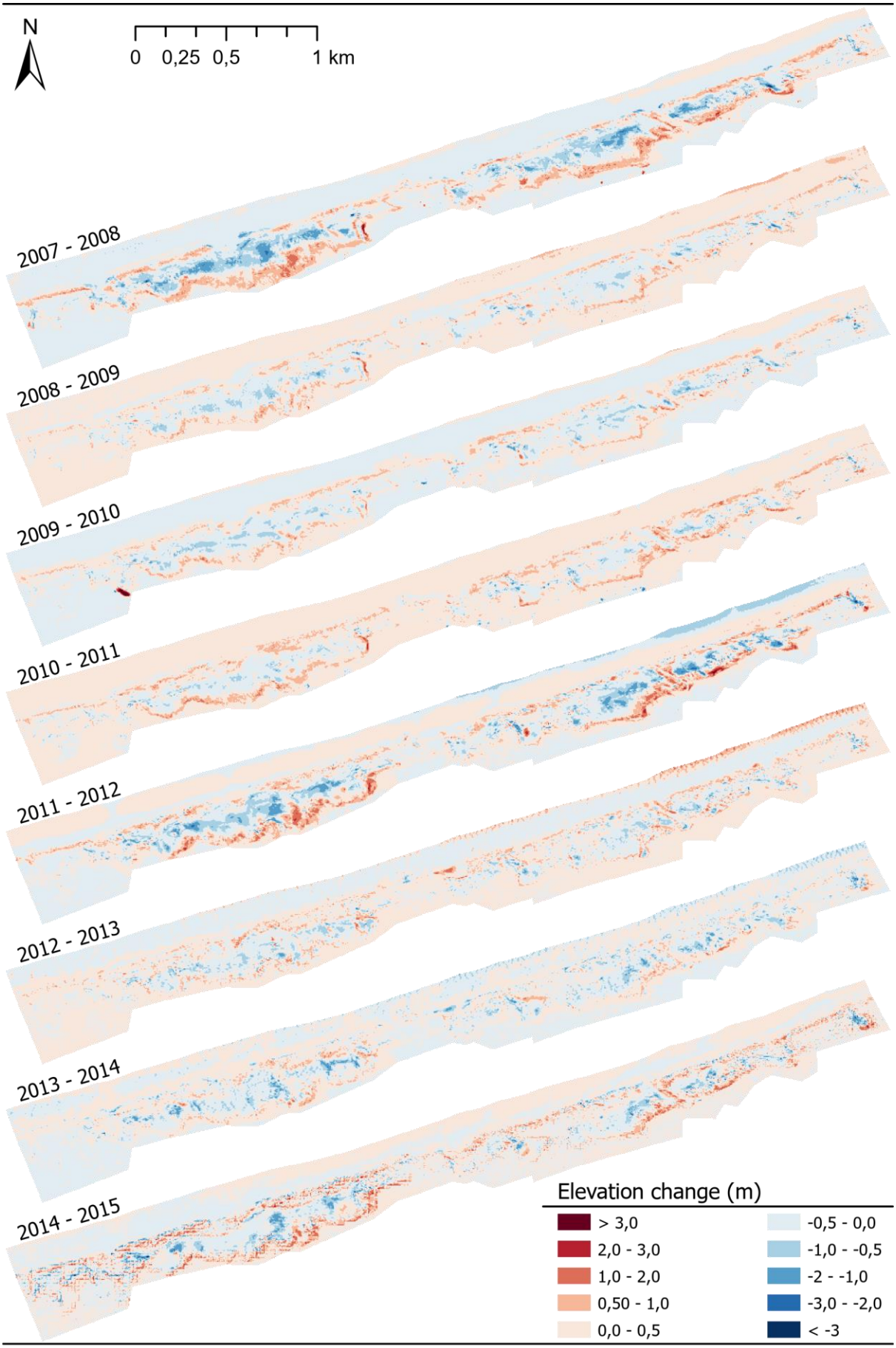
N
0 0,25 0,5 1 km
2007 - 2008
2008 - 2009
2009 - 2010
2010 - 2011
2011 - 2012
2012 - 2013
2013 - 2014
2014 - 2015
Elevation change (m)
> 3,0
2,0 - 3,0
1,0 - 2,0
0,50 - 1,0
0,0 - 0,5
-0,5 - 0,0
-1,0 - -0,5
-2 - -1,0
-3,0 - -2,0
< -3

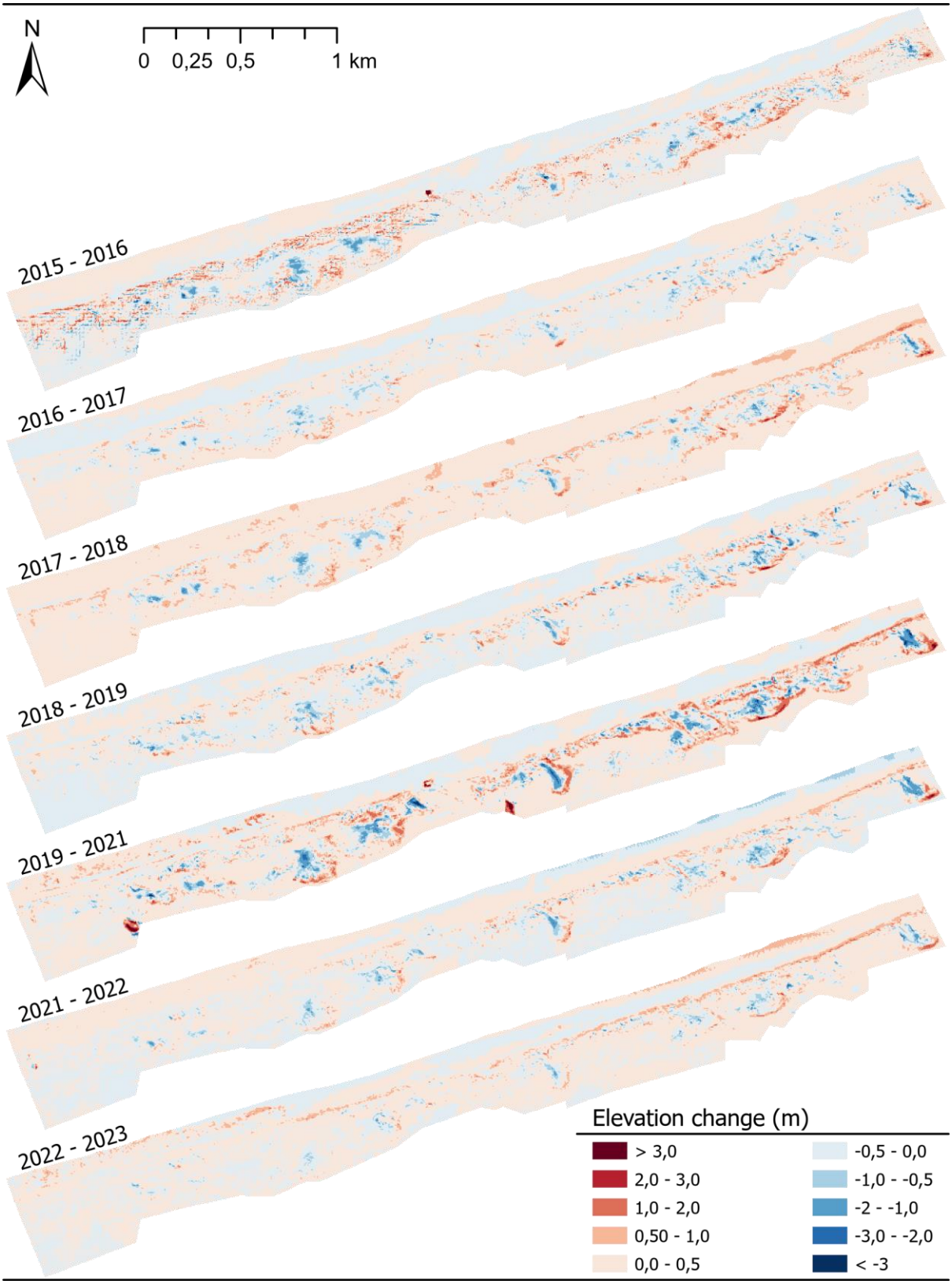

Appendix 3. Elevation difference models with blue colours indicating a decrease in elevation (erosion) and red colours indicating an increase in elevation (deposition). Although most models show a one-year elevation change, several models show a two-year elevation changes due to missing or incomplete data.

Appendix 4. Geometries of computed blowout surface areas

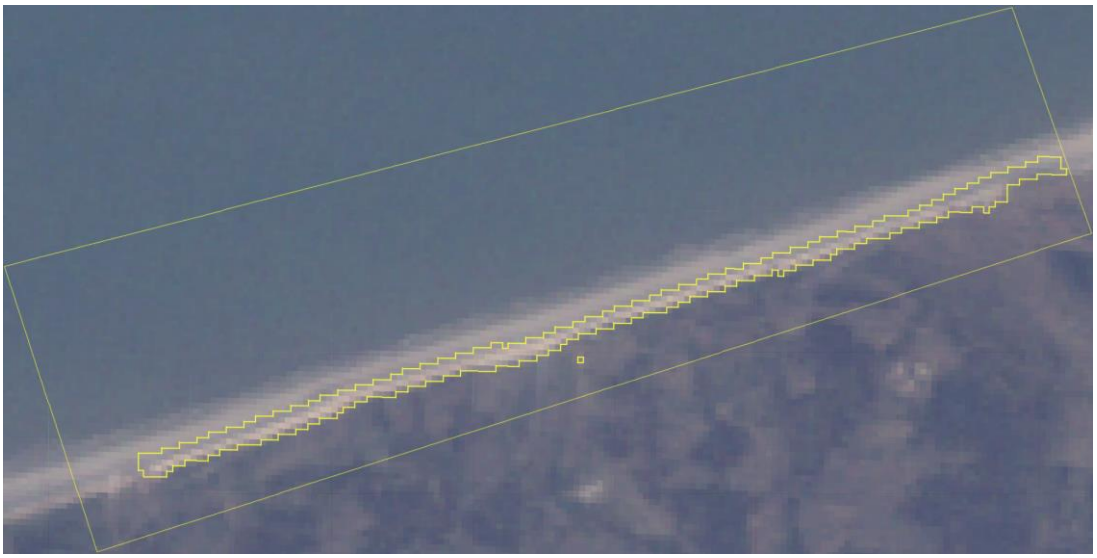

19 March 1986. Landsat-5. SSA: 482.564 m^2

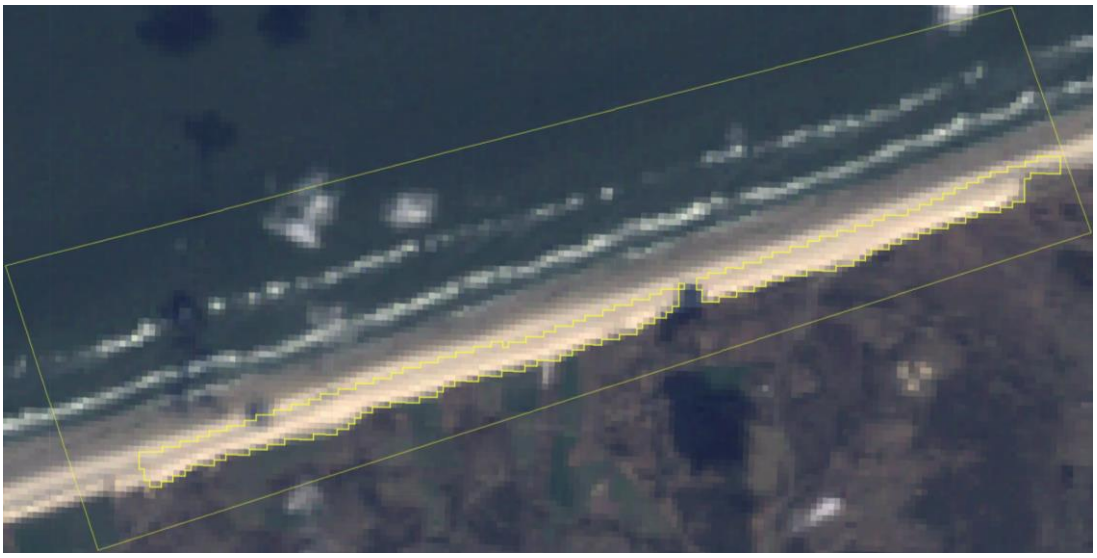

08 April 1990. Landsat-5. SSA: 722.082 m^2

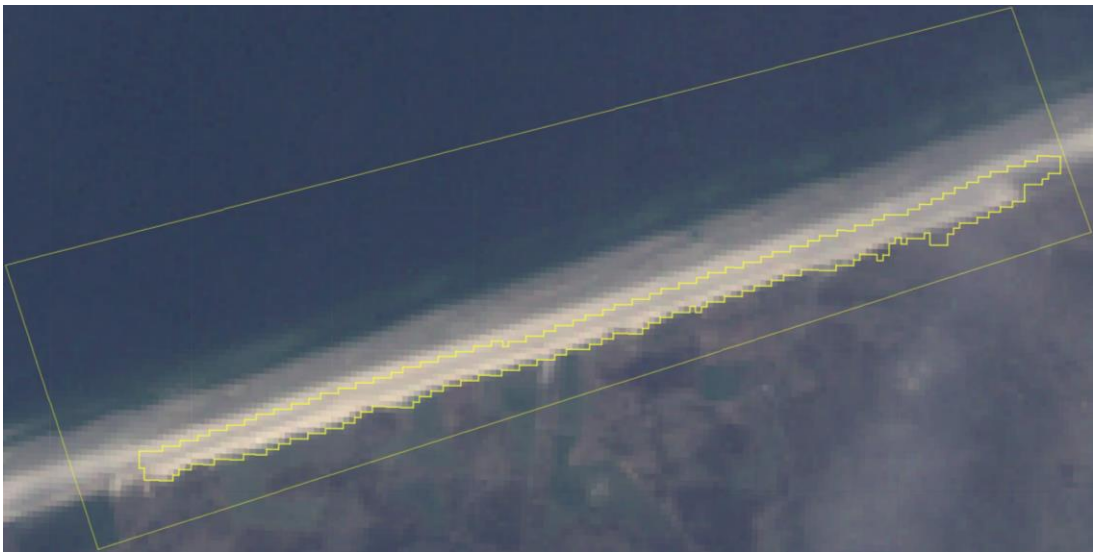

16 April 1993. Lansdat-5. SSA: 771.315 m^2

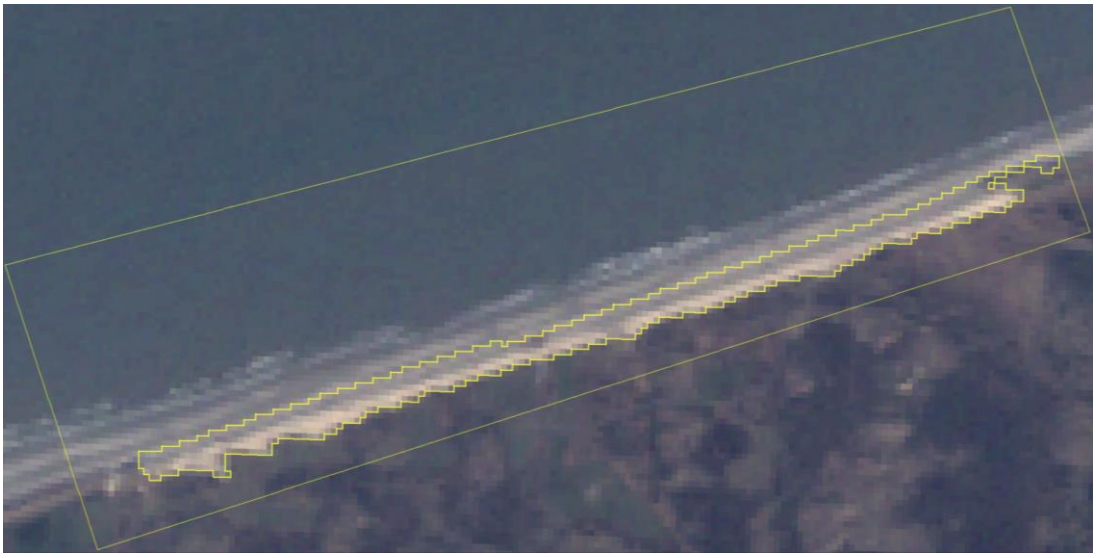

1 March 1997. Landsat-5. SSA: 772.565 m²

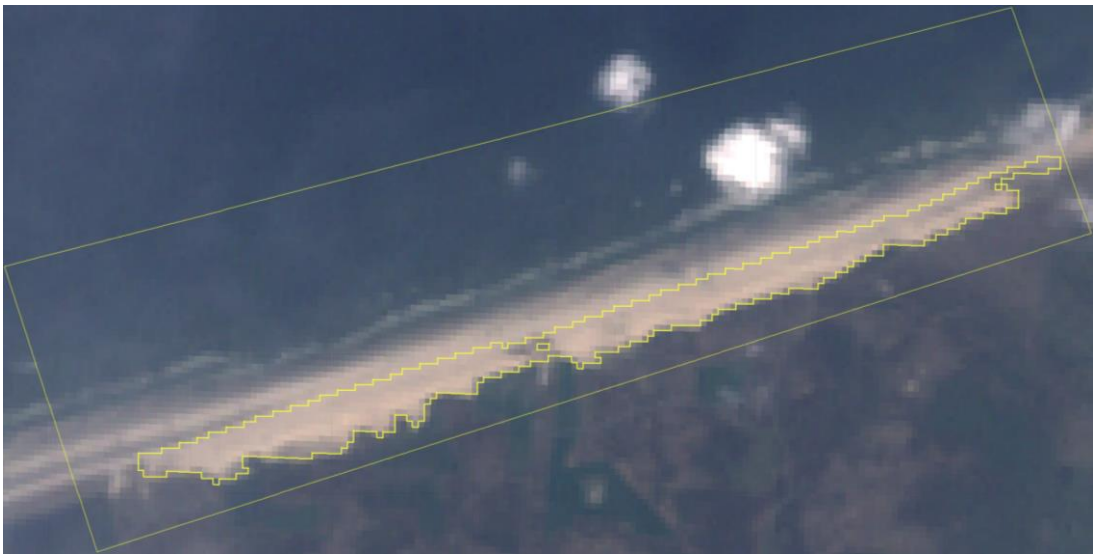

27 April 2000. Landsat-7. SSA: 927.330 m²

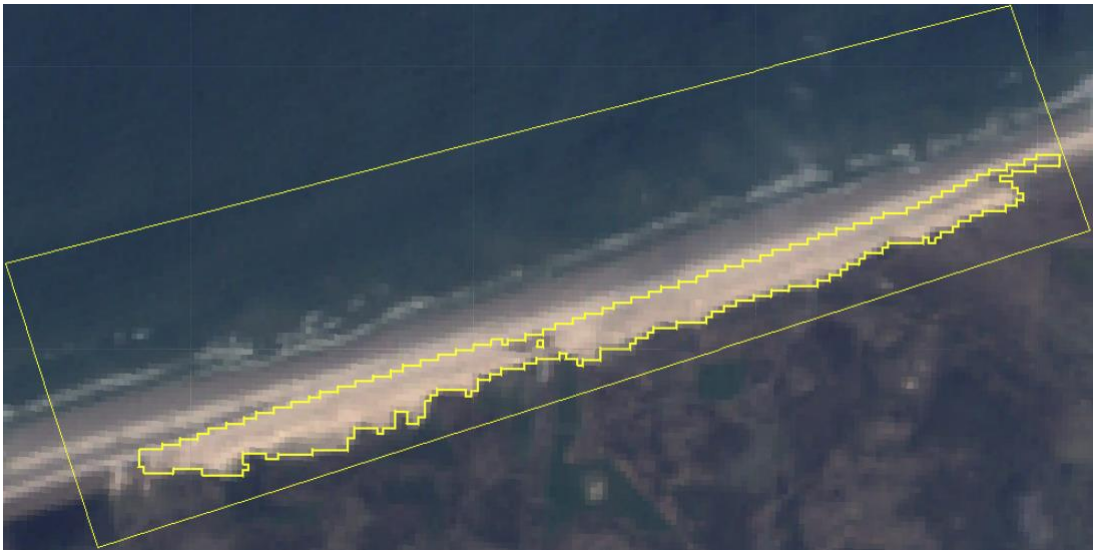

29 March 2004. Landsat-5. SSA: 1.019.867 m²

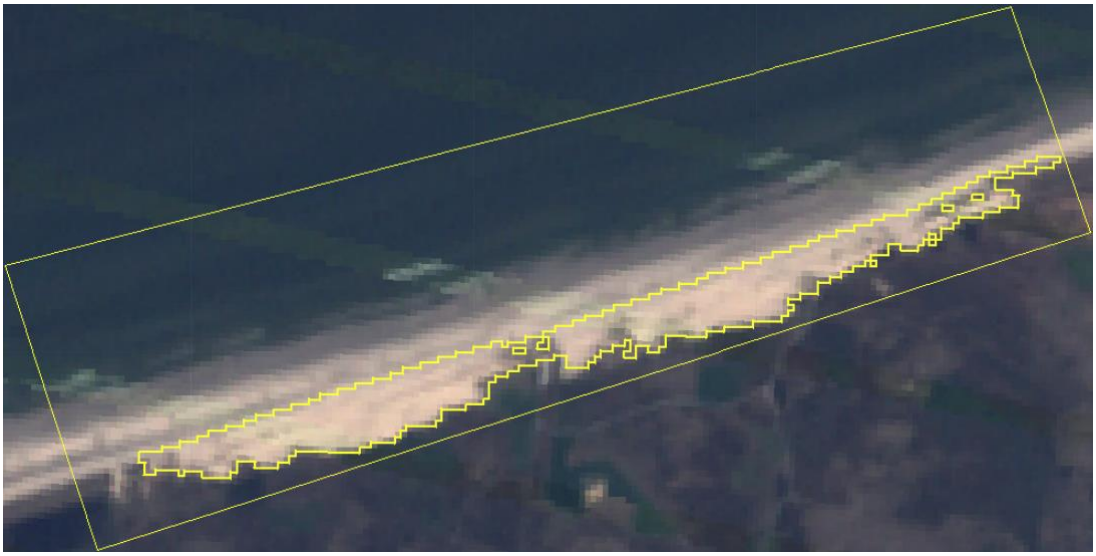

15 April 2007. Landsat-7. SSA 1.074.550 m²

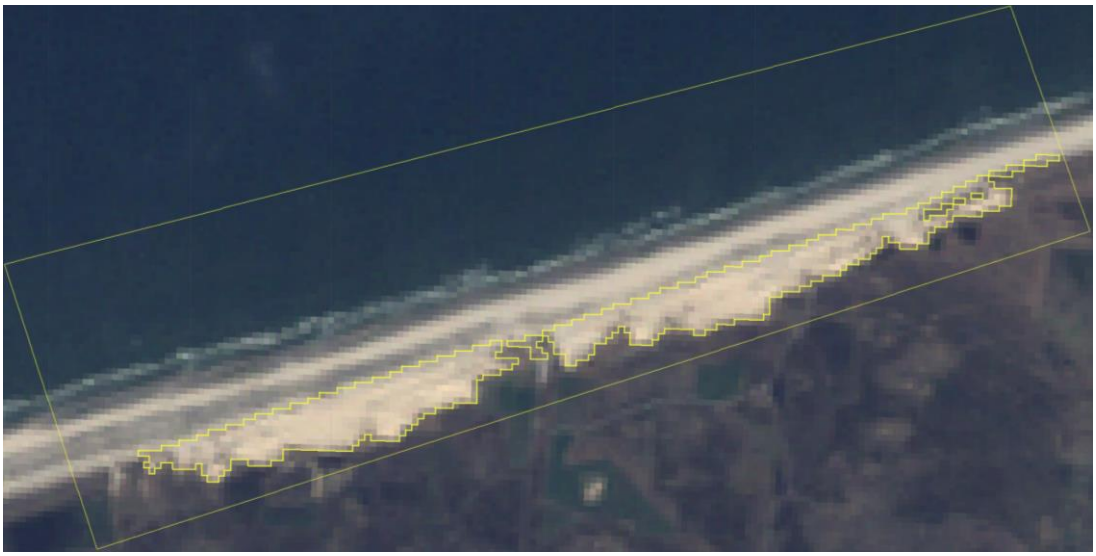

15 April 2010. Landsat-5. SSA: 963.093 m²

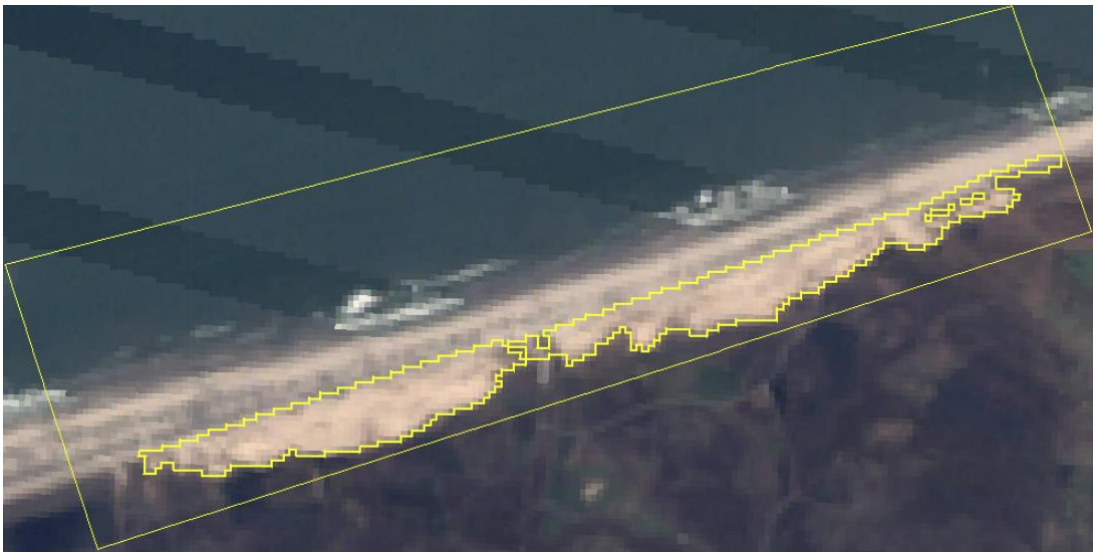

22 April 2013. Landsat-7. SSA: 1.043.984 m²

16 March 2014. Landsat-8. SSA: 1.040.182 m²

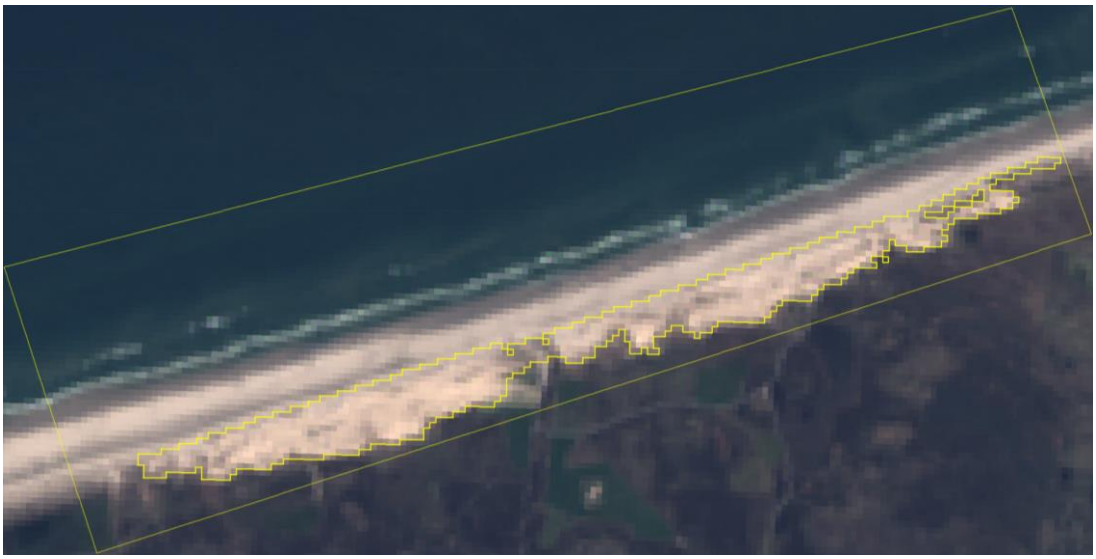

20 April 2015. Landsat-8. SSA: 1.053.462 m²

01 April 2016. Sentinel-2A. SSA 1.043.161 m²

13 April 2017. Sentinel-2A. SSA 936.898 m²

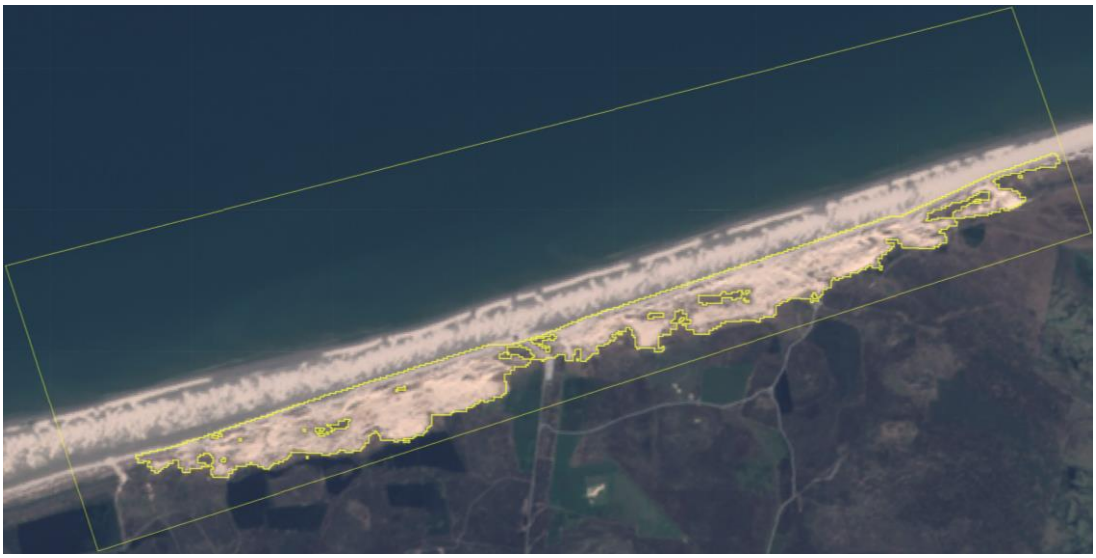

18 April 2018. Sentinel-2A. SSA 997.968 m²

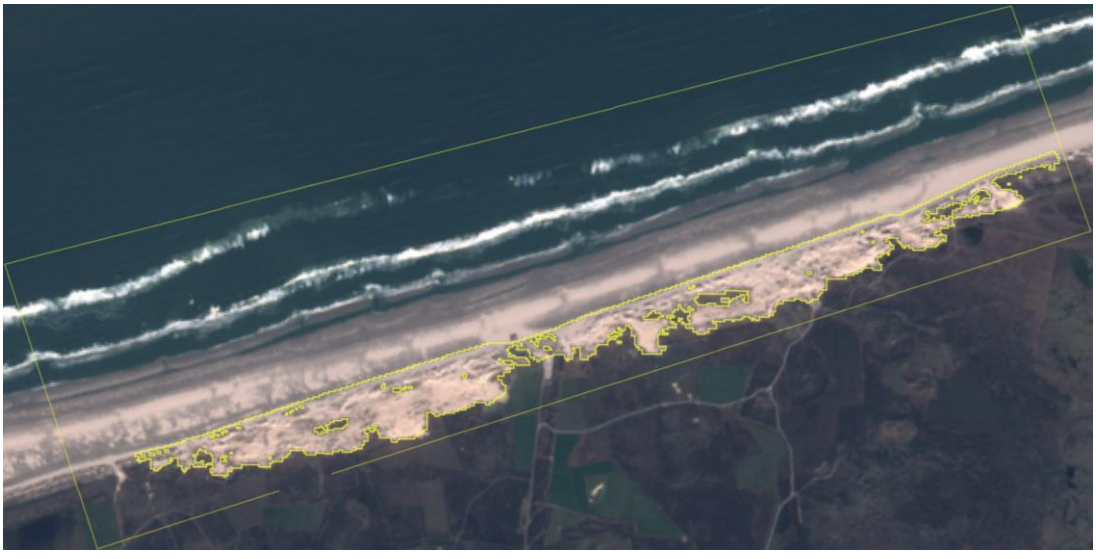

1 April 2019. Sentinel-2B. SSA: 1.008.257 m²

5 April 2020. Sentinel-2B. SSA: 1.011.224 m²

31 March 21. Sentinel-2B. SSA: 889.923 m²

2 April 22. Sentinel-2B. SSA: 861.556 m²

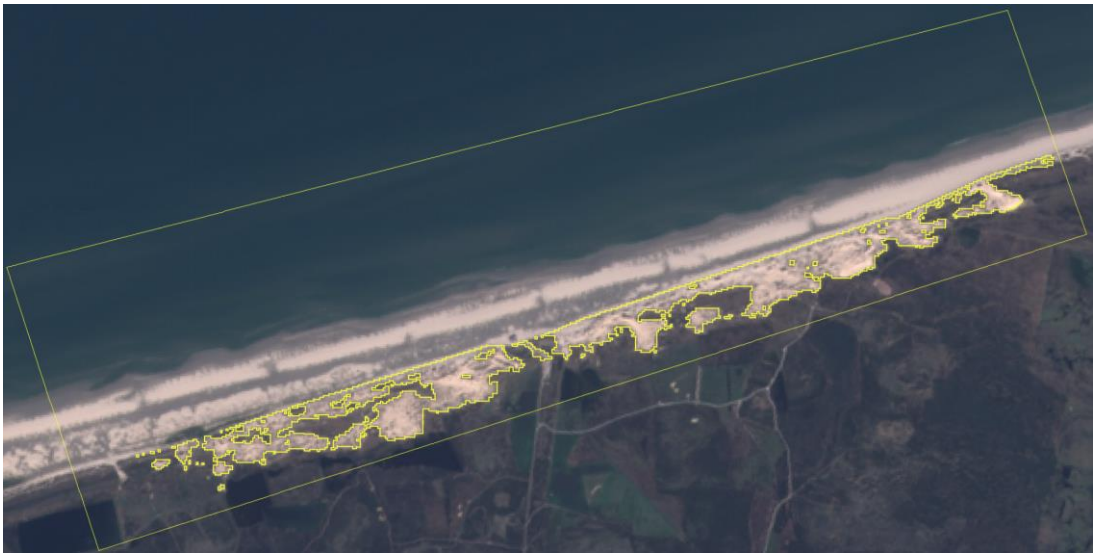

5 April 2023. Sentinel-2A. SSA: 715.579 m^2

Appendix 4. Geometries of computed sand surface areas (SSA) from collected satellite imagery from either April or March.